01 Aug 2022

Coupled Effect of Fiber and Granular Skeleton Characteristics on Packing Density of Fiber-Aggregate Mixtures

Naimeh Nouri

Masoud Hosseinpoor

Ammar Yahia

Kamal Khayat
Missouri University of Science and Technology, khayatk@mst.edu

Recommended Citation

Coupled effect of fiber and granular skeleton characteristics on packing density of fiber-aggregate mixtures

Naimeh Nouri [a], Masoud Hosseinpoor [a,*], Ammar Yahia [a], Kamal H. Khayat [b]

[a] *Université de Sherbrooke, Department of Civil and Building Engineering, Sherbrooke, Québec, Canada*
[b] *Missouri University of Science and Technology, Center for Infrastructure Engineering Studies, Department of Civil, Architectural and Environmental Engineering, Rolla, MO, USA*

ARTICLE INFO

ABSTRACT

The addition of fiber to cementitious materials enhances mechanical performance but can reduce workability of the fiber-reinforced concrete (FRC) mixtures. This can be due to the negative effect of fibers on packing density (PD) of the fiber-coarse aggregate (F-A) combination. The performance of FRC, as a diphasic suspension, is dependent on the characteristics of both F-A (suspended-solid skeleton) and mortar (suspending liquid) phases. PD can reflect the voids within the F-A skeleton to be filled with mortar. An adequate optimization of the characteristics of the F-A skeleton can modify the performance of FRC in fresh and hardened states. The F-A skeleton can be characterized in terms of particle-size distribution, volumetric content, and morphology of the coarse aggregate, as well as size, rigidity, and content of fibers. In this study, a comprehensive investigation was undertaken to identify the coupled effect of the characteristics of fibers and coarse aggregate on the PD of F-A combination used without any cement paste/mortar. The solid components play a key role in the overall performance of the concrete produced. This study was carried out to optimize the F-A combination and enhance the workability design of FRC. Various types of steel, polypropylene, and polyolefin fibers having different sizes and rigidities were investigated. Moreover, four combinations of three different classes of coarse aggregate were used to proportion F-A mixtures. Test results showed that shorter length, smaller diameter, and more flexible fibers can lead to higher PD of F-A systems. Moreover, the coarser aggregate skeleton with larger interparticle voids led to more available length for fibers to be deformed, hence improving the PD of F-A mixtures. New empirical models were proposed to predict the packing density of F-A combinations given the characteristics of coarse aggregate and fibers, as well as the level of compaction. The established models were employed to propose a new proportioning approach for fiber-reinforced self-consolidating concrete mixtures to achieve the targeted workability.

1. Introduction

Hardened cement-based materials are brittle because of their low tensile strength and strain capacity. The addition of fibers can enhance the tensile, flexural, and ductility properties of fiber-reinforced concrete (FRC) [1–3]. However, adding fibers can negatively affect the workability of FRC. This can be due to fiber-aggregate interaction, hence forming blocking arches in vicinity of obstacles. The negative effect of fibers on workability of FRC depends on content, size (length and diameter), type, and rigidity of fibers [4–6]. From workability point of view, there is a critical content of fibers above which concrete is not flowable anymore and fiber clumping can occur [6–9]. This critical

content decreases for larger and rigid fibers. Khayat et al. [10] investigated the effect of fiber characteristics on workability of fiber-reinforced self-consolidating concrete (FR-SCC). The authors optimized FR-SCC mixtures by keeping the average mortar thickness constant to achieve a given workability. This average thickness is function of surface area of aggregate and fibers, as well as the interparticle voids. The packing density (PD) of solid skeleton can reflect the amount of cement paste required to fill the interparticle voids. Higher packing density leads to more excess paste available to cover fibers and aggregate, hence increasing the workability of FR-SCC.

In order to design FR-SCC with adequate properties, the influence of various effective parameters should be considered simultaneously.

Table 1
Proportioning of investigated coarse aggregate mixtures.

Application	Coarse aggregate mixtures	CA1 (%)	CA2 (%)	CA3 (%)	PD_A	D_A (mm)	AV_A (m²/m³)
Precast	MSA20-1	45	50	5	0.560	12.748	737.656
	MSA20-2	30	55	15	0.555	13.139	682.292
	MSA20-3	15	60	25	0.547	13.516	626.929
	MSA20-4	–	65	35	0.545	13.880	571.565
Repair	MSA14-1	100	–	–	0.558	12.595	860.295
	MSA14-2	80	20	–	0.560	12.596	820.313
	MSA14-3	60	40	–	0.561	12.598	780.332
	MSA14-4	40	60	–	0.562	12.599	740.350
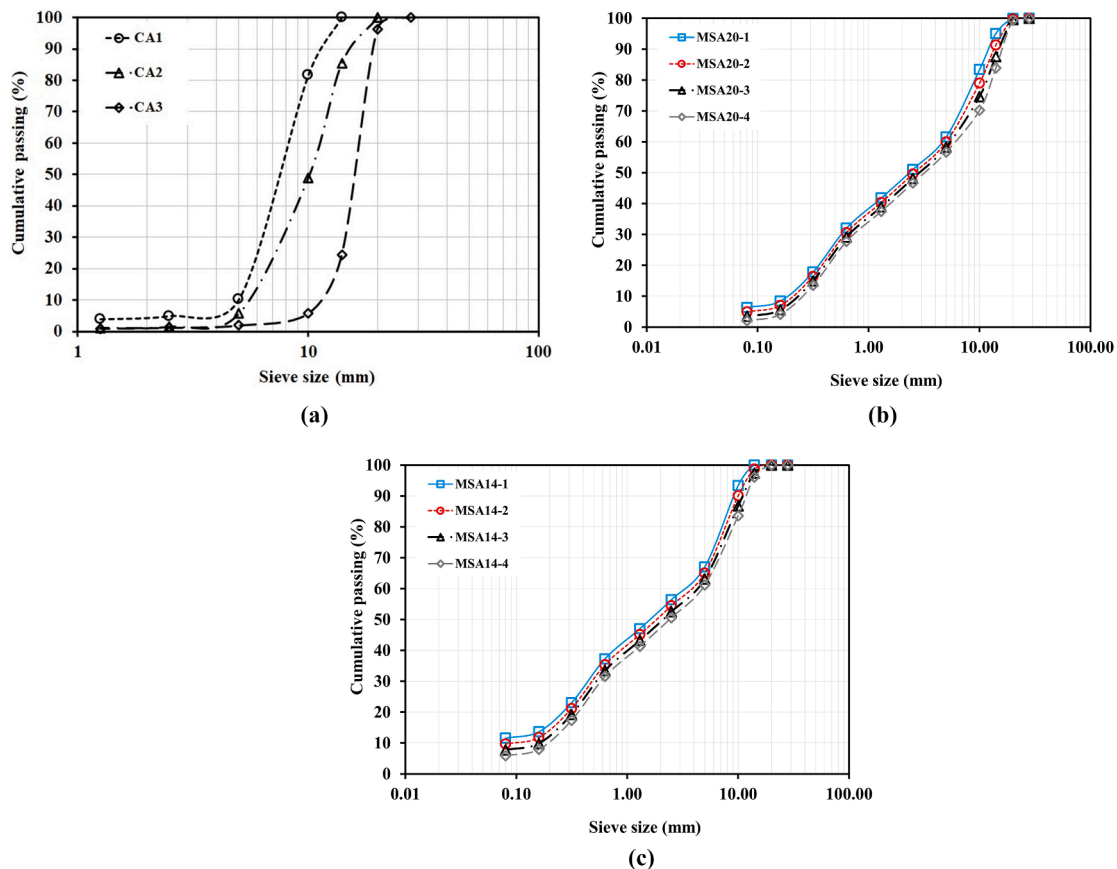
Fig. 1. Particle-size distributions of (a) investigated coarse aggregate, and coarse aggregate mixtures for (b) precast (MSA20) and (c) repair (MSA14) applications.

Hosseinpoor et al. [11,12] evaluated the coupled effect of characteristics of aggregate, coarser than 1.25-mm diameter, and rheological properties of suspending fine mortar (<1.25 mm) on stability and passing ability of self-consolidating concrete (SCC). The authors reported that the ratio of the volumetric content-to-packing density (φ/PD) of coarse aggregate shows a dominant effect on homogeneous performance of SCC during flow, and thereafter at rest. Koura et al. [13] showed that the optimization of the paste volume and φ/PD ratio are effective parameters on dynamic stability of SCC rather than the rheology of paste (i.e., water-to-binder ratio and high-range water-reducer (HRWR) dosage). On the other hand, Mehdipour and Libre [6] evaluated the effect 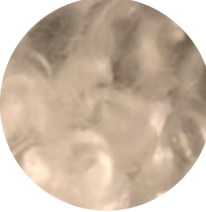of volumetric content and rigidity of polypropylene (PP) and glass fibers (GF) on PD of FR-SCC. They reported that increasing fiber content, especially rigid GF, up to a certain point slightly decreased the PD, beyond which PD of fibers and solid particles drastically decreases. Kwan et al. [14] reported that when fiber content is greater than the one required to fill the interparticle voids, leading to lower PD, the probability of fiber agglomeration can increase.

Although, various studies were carried out to evaluate the effect of fiber characteristics on workability and mechanical properties of concrete [15], limited information exists regarding the correlation between the fiber characteristics, packing density of solid skeleton, and workability of FRC. Aggregate characteristics, including particle-size distribution (PSD) and morphology, can also significantly affect the packing density of solid skeleton (i.e., fiber and aggregate combination) [16–22]. It was revealed that the use of a wide range of PSD shows positive effect on packing density of granular skeleton where the finer particles, up to an optimum content, can fill the voids between the coarser ones, hence increasing the PD [15]. Hafid et al. [22] reported the significant effect of fine particles' morphology (e.g., aspect ratio) on packing density of solid skeleton. The authors employed two different methods, including loose- and random dense-packing methods. It was revealed that vibration and external compaction can significantly change the arrangement of aggregate, hence affecting the PD values. Martinie et al. [23] reported the effect of duration and intensity of vibration on loose- and dense-PDs of fibers. Chu et al. [24] showed that without adequate compaction

Table 2
Physical characteristics of investigated fibers.

Fiber type	Macro steel	Micro steel	PPF	PSI	TUF	IT	ST
Material	Steel		Polypropylene		Polyolefin		
S.G.	7.85	7.80	0.91	0.91	0.91	0.91	0.91
L_f (mm)	30	13	38	19	38	55	42
D_f (mm)	0.55	0.20	0.39	0.12	0.69	0.92	0.79
A.R.	55	65	97	156	55	60	53
E (GPa)	200	203	3.5	–	9.5	3.9	3.9

S.G.: Specific gravity.
L_f: Fiber length.
D_f: Fiber diameter.
A.R.: Aspect ratio.
E: Modulus of elasticity.

where the fibers are not yet deformed, the PD of F-A skeleton depends only on the size and rigidity of fibers.

Few studies were carried out to predict the coupled effect of different contents and types of fibers, as well as PSD of aggregate on PD of F-A. Chu et al. [24] investigated the effect of rigid fibres on PD of F-A mixtures for different contents (0–2%) and types of rigid-steel fibers of 30- and 60-mm length, as well as various classes of aggregate (0.6–20 mm). The authors reported that increasing the content and size of fibers led to lower PD of F-A combination, especially in presence of coarse aggregate with higher maximum size (i.e., 20 mm). Using the compressible packing model (CPM), de Larrard [25] reported similar conclusions for mixtures containing rigid-steel fibers and fine and coarse aggregate. However, the proposed CPM model was not validated for flexible fibers. On the other hand, the CPM model was not established to predict the loosely-packed PD (LPD) of F-A, which can more accurately describe the packing state of F-A skeleton in concrete matrix through the mixing process and low casting rates. Actually, during the mixing process, where there is no adequate compaction, fibers are not deformed yet. Therefore, the F-A system is in loose state and the LPD should be taken into consideration. However, in the case of transportation and casting processes, such as shotcrete and highly-pressure pumping, where a higher level of compaction applies on the F-A system, fibres can deform [26,27]. Therefore, the densely-packed PD (DPD) can more properly simulate the packing state of the F-A skeleton.

In this study, the coupled effect of fiber and coarse aggregate characteristics, including the volumetric content, length, diameter, and rigidity of different flexible and rigid fibers, as well as the PD and size of coarse aggregate on LPD and DPD of F-A combinations were evaluated. Accordingly, three classes of coarse aggregate with different PSDs were mixed with various volumetric fractions of rigid and flexible fibers. The LPD and DPD of the investigated F-A mixtures were evaluated without any compaction and under a given gyratory compaction, respectively. New empirical models were then established to predict the packing density of F-A mixtures under different levels of compaction. A new workability-design approach for fiber-reinforced self-consolidating concrete (FR-SCC) mixtures was then proposed based on the established LPD and DPD models.

2. Experimental study

Three different classes of crushed limestone coarse aggregate of 5–10 mm (CA1), 5–14 mm (CA2), and 5–20 mm (CA3) were used. The specific gravity values of the CA1-3 coarse aggregate are 2.72, 2.73, and 2.76, respectively. Two different groups of F-A mixtures were proportioned with the maximum-size aggregate (MSA) of 20 mm (MSA20) and 14 mm (MSA14). Each MSA20 and MSA14 series were proportioned using four different combinations (MSA20-1 to MSA20-4 and MSA14-1 to MSA14-4) of CA1-3 coarse aggregate to achieve wide ranges of PSD. It is worthy to mention that the MSA20 and MSA14 mixtures correspond to those used in precast and repair applications, respectively. The volumetric proportioning, packing density (PD_A), PSD, average diameter (D_A), and the total surface area-to-unit volume (AV_A) of the investigated coarse aggregate mixtures are summarized in Table 1 and Fig. 1. It is worth mentioning that D_A and AV_A of each coarse aggregate combination were evaluated using the three-dimensional morphological analyses and PSD of different classes of coarse aggregate. As reported by Hosseinpoor et al. [11,12,28,29], several samples of different subclasses of coarse aggregate, corresponding to different successive standard sieves, were scanned using a 3D laser scanner. The larger and smaller sides of the minimum bounding rectangles of 2D projections of the 3D scanned particles, corresponding to their maximum (D_{max}) and minimum (D_{min}) diameters, respectively, were determined for each subclass of coarse aggregate. The mean diameter of each coarse aggregate subclass ($\overline{D}_i$) was calculated using the average of D_{max} and D_{min} values. Furthermore, the ratio of 3D surface area-to-volume of each coarse

Fig. 2. Procedure of PD measurements, including (a) weighting different coarse aggregate classes, (b) homogenizing coarse aggregate, (c) adding fibers to coarse aggregate, (d) homogenizing F-A mixture, (e) ICT set-up, (f) layer-by-layer filling of cylindrical specimen, and (g) flattening the specimen's top surface.

aggregate subclasses (AV_i) was determined using the 3DSmax software. Considering the PSD of the investigated coarse aggregate combinations, the D_A and AV_A values were determined using the arithmetic average of mean diameter $\overline{D}_i$ and AV_i values, respectively.

Different types of steel fibers were mixed with both MSA20 and MSA14 coarse aggregate mixtures. Different types of synthetic fibers were also mixed with the MSA14 mixtures, corresponding to concrete repair applications. Two different macro- and micro- rigid fibers with different sizes, including the hooked-end macro and straight-micro steel fibers, were investigated. Moreover, the flexible-synthetic fibers included three types of polypropylene fibers, including PPF, TUF, and PSI fibers, as well as two types of polyolefin fibers, including macro-IT and micro-ST fibers. The physical characteristics of the investigated fibers are summarized in Table 2.

The experimental program was divided into two phases. The first phase was undertaken to evaluate the effect of fiber size, rigidity, and volume as well as coarse aggregate characteristics on packing density of the F-A combination (sections 3.1 to 3.4). In total, 216 F-A mixtures were proportioned with six fiber volumes (V_f) of 0.4%, 0.5%, 0.6%, 0.7%, 0.8%, and 0.9% mixed with eight coarse aggregate mixtures of MSA-14 and MSA-20 (Table 1).

First, the required coarse aggregate (Table 1) and fiber samples needed to achieve a total solid volume ($V_f + V_{CA}$) of 0.6 L were weighted. The coarse aggregate sample (Fig. 2a) was manually mixed for 5 min to ensure a homogeneous mixture (Fig. 2b). The fibers were separated manually and then added to the coarse aggregate (Fig. 2c). The F-A mixture was manually mixed for 5 min to ensure homogeneous dispersion (Fig. 2d). The PD of the coarse aggregate (PD_A) (Table 1) and F-A mixtures were determined using the Intensive Compaction Tester (ICT) (Fig. 2e) [30–32]. The testing sample consisted of a cylindrical specimen measuring 100-mm diameter and 200-mm height. The F-A mixture was introduced in the cylindrical container in three equal layers (Fig. 2f) to ensure vertical homogeneity of the samples. The top surface

of the samples was then leveled (Fig. 2g) before subjecting them to the compaction load. A constant normal pressure of 20 kPa was exerted on the top of the cylindrical specimen, and a gyratory motion is applied to induce shear stress [30–32]. The low applied normal pressure was selected to avoid aggregate crushing. In total, 50 gyratory cycles with a gyration angle of 40 mrad were applied, and the tests were repeated three times for each sample. The LPD and DPD values were evaluated after 4 and 50 gyratory cycles, respectively.

The PD was calculated as the ratio of the bulk density of the investigated F-A samples after a given number of cycles to their corresponding density value (ρ_{FA}). The ρ_{FA} values were calculated by the volumetric-weighted arithmetic mean of densities of the fiber and coarse aggregate in each mixture. The volume of fiber and coarse aggregate were calculated by dividing their mass weighted for each sample to their corresponding density values. The reported PD values correspond to the average determined on three different measurements. It is worth mentioning that in the case of LPD, no deformation was observed in the fibers, due to low level of compaction. The LPD values were thus dependent only on the size (i.e., diameter and length) and fiber volume and coarse aggregate characteristics. However, after applying 50 gyratory cycles, the fibers were deformed. Therefore, the difference between the DPD and LPD values can reflect the effect of fibers' rigidity. Accordingly, the effect of volume and size of fibers, as well as coarse aggregate characteristics were evaluated using the LPD values. Moreover, the relative DPD-to-LPD values were investigated to evaluate the effect of fiber rigidity on DPD of F-A mixtures.

The empirical models are then established to predict the packing density of F-A mixtures as function of fiber-coarse aggregate characteristics in the second phase. In the case of the LPD model (further discussed in the section 3.5.1), 126 F-A mixtures were randomly selected and investigated. Furthermore, additional 34 mixtures were proportioned with PPF, TUF, ST, and IT fiber volumes ranging from 0.4% to 1.77% and different PSDs of MSA 14-1, MSA14-2, MSA 14-3, and MSA

Table 3
Proportioning of the FR-SCC mixtures made with macro steel fiber.

Application	Mix	Binder (kg/m³)	w/b	Paste volume (%)	Sand (0–5 mm) (kg/m³)	PSD of coarse aggregate	CA1 (kg/m³)	CA2 (kg/m³)	CA3 (kg/m³)	Fiber (kg/m³)	V_f in F-Amixture (%)	HRWR (ml/100 kg of binder)	Slump flow (mm)
Repair	R1	352	0.42	27	999	MSA14-1	825	–	–	22	0.9	3300	667
	R2	352		27	999	MSA14-2	661	166	–	17	0.7	2860	665
	R3	352		27	999	MSA14-3	497	333	–	9	0.4	2600	662
	R4	392		30	955	MSA14-1	789	–	–	20	0.9	1500	700
	R5	392		30	955	MSA14-2	632	159	–	16	0.7	1350	673
	R6	392		30	955	MSA14-3	475	318	–	9	0.4	1180	656
	R7	431		33	910	MSA14-1	752	–	–	20	0.9	1140	678
	R8	431		33	910	MSA14-2	603	151	–	15	0.7	980	685
	R9	431		33	910	MSA14-3	454	303	–	9	0.4	820	694
Precast	P1	474	0.35	33	910	MSA20-4	–	493	268	9	0.4	1070	683
	P2	474		33	910	MSA20-2	226	416	115	15	0.7	1070	678
	P3	474		33	910	MSA20-3	113	455	192	11	0.5	1070	694
	P4	503		35	881	MSA20-4	–	477	260	8	0.4	965	678
	P5	503		35	881	MSA20-2	219	403	111	15	0.7	965	695
	P6	503		35	881	MSA20-3	110	440	185	11	0.5	965	697
	P7	532		37	852	MSA20-4	–	461	251	8	0.4	870	694
	P8	532		37	852	MSA20-2	211	389	107	14	0.7	870	690
	P9	532		37	852	MSA20-3	106	425	179	10	0.5	870	695
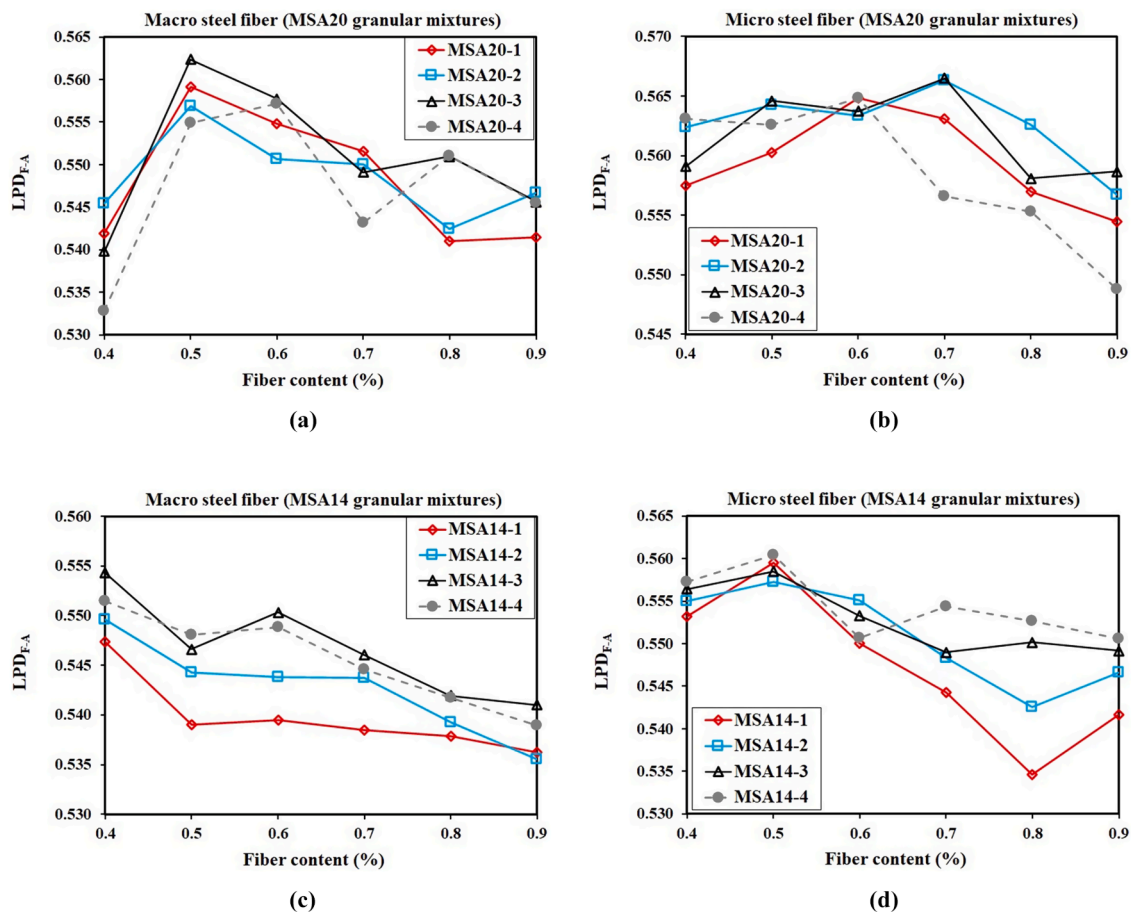
Fig. 3. Variation of the LPD values of F-A mixtures with fiber content, including (a) macro fiber and MSA20, (b) micro steel fiber and MSA 20, (c) macro steel fiber and MSA14, and (d) micro steel fiber and MSA14.

14-4 to validate the established model (section 3.5). Moreover, the DPD model (section 3.5.2) was established based on randomly selected 127 mixtures, proportioned with 0.4%–1.77% volumetric contents of rigid (macro and micro steel) and semi-rigid (IT and ST polyolefin) fibers, as well as eight different PSDs of coarse aggregate mixtures, presented in

Table 1. The established DPD model is then validated using 100 additional F-A mixtures. These include 29 remaining reference F-A mixtures in addition to 71 F-A mixtures extracted from some empirical tests on 18 FR-SCC mixtures made with a ternary cement (TerC³), volumetric sand (0–5 mm)-to-total aggregate ratio of 55%, and macro steel fibers.
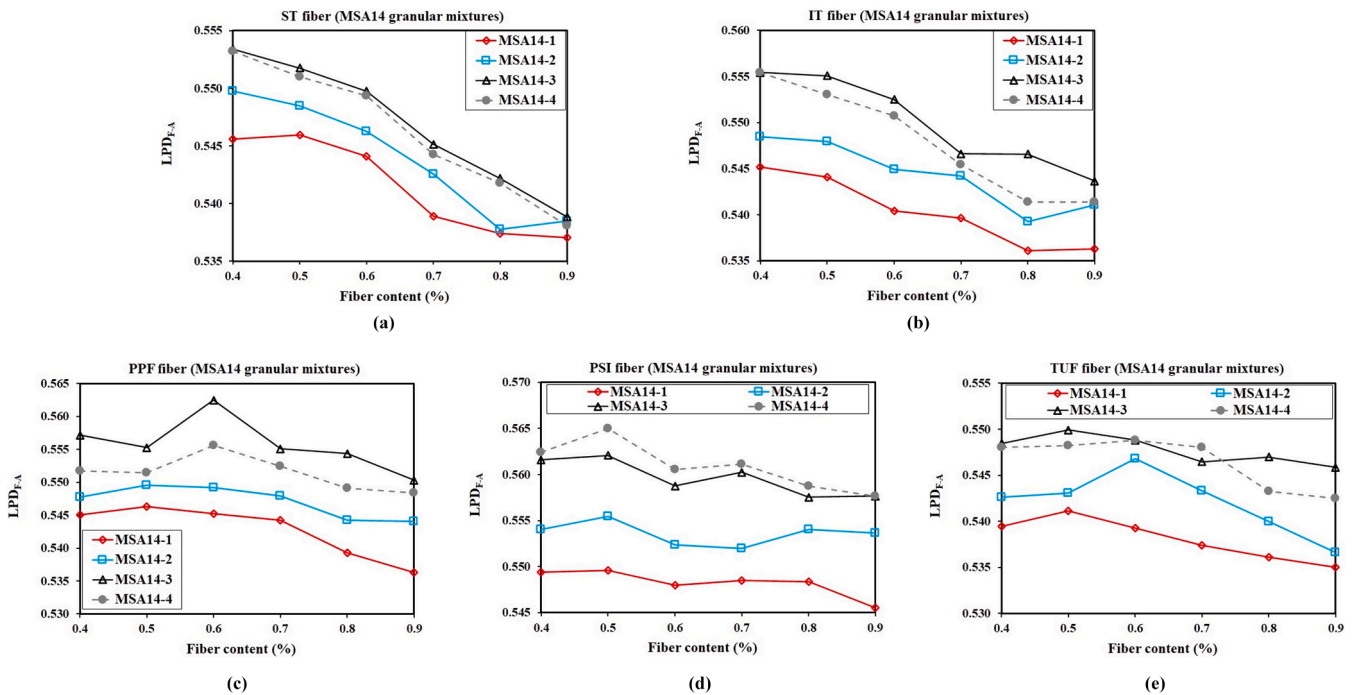
Fig. 4. Variation of LPD of F-A mixtures with synthetic fiber volume for: (a) ST, (b) IT, (c) PPF, (d) PSI, and (e) TUF fibers with MSA14 coarse aggregate mixtures.
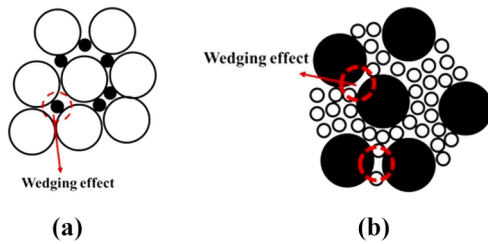

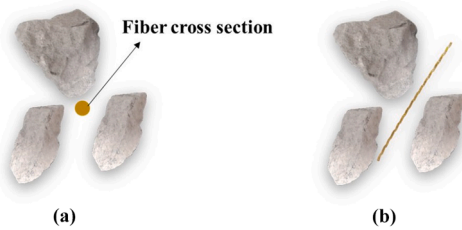**Fig. 5.** Wedging effect in (a) coarser and (b) finer PSD of aggregate [15].

Fig. 6. (a) Cross-sectional and (b) longitudinal placement of fibers between aggregate.

In the case of mixtures that can be used for repair applications, 9 FR-SCC mixtures were made with MSA14 coarse aggregate mixtures and paste volumes of 0.27, 0.30, and 0.33 and water-to-binder ration (w/b) of 0.42. On the other hand, 9 FR-SCC mixtures for precast application made with MSA20, paste volumes of 0.33, 0.35, and 0.37, and w/b of 0.35 were investigated. The FR-SCC mixtures were prepared with a polycarboxylate-based HRWR to achieve a slump flow of 680 ± 20 mm (Table 3). The FR-SCC mixtures were tested using the L-Box [10] and T-Box [13] tests to evaluate their passing ability and dynamic stability, respectively. Various cylindrical samples measuring 100 mm × 200 mm were taken from two lateral sections of the investigated L-Box and T-Box set-ups. These included samples from behind the rebars in the vertical

compartment of the L-Box and at the end of the L-Box channel, as well as the tilt-up and tilt-down zones of the T-Box test, using the method described in references [11–13]. In total, 71 concrete samples mixtures were wet-sieved on 5-mm sieve and dried to extract their F-A portions. The volumetric content of macro steel fibers and coarse aggregate in the extracted F-A samples were measured by separating the fibers using a magnet. The LPD and DPD values of the extracted F-A samples were then determined.

3. Results and discussions

3.1. Effect of fiber content on LPD of F-A mixtures

As can be observed in Fig. 3, in the case of macro and micro steel fibers, the LPD of F-A mixtures generally increased with fiber content up to an optimum value before decreasing. For example, in the case of MSA20-3 coarse aggregate mixture, increasing the macro and micro steel fibers' content up to 0.5% and 0.7% resulted in 3.91% and 1.24% increase in the LPD, respectively. It is worthy to mention that the incorporation of macro-steel fibers resulted in a decrease in LPD of F-A combinations proportioned with MSA14 coarse aggregate mixtures, regardless of the fiber content.

Furthermore, the effect of synthetic fibers on the LPD of F-A mixtures is illustrated in Fig. 4. As can be observed in Fig. 4a and 4b, increasing ST and IT fiber content led to decrease in LPD of F-A mixtures. On the other hand, as shown in Fig. 4c-e, the LPD of F-A mixtures containing PP fibers (i.e., PPF, PSI, and TUF) slightly increased by increasing the fiber content up to a certain value, beyond which the LPD values decreased. This can be explained by similar phenomenon causing loosening, wedging, and wall effects in mixture containing sand and coarse aggregate [15,27]. Loosening effect happens when finer particles are added in the space between coarser aggregate. Accordingly, adding finer aggregate led to increase in packing density of the F-A mixture (Fig. 5a). However, when the maximum packing density is achieved, increasing the volume of finer particles beyond an optimum content can disturb the packed array of the coarser aggregate skeleton and reduced the packing density of the F-A mixture. Moreover, although some finer particles fill the interparticle voids, other fine aggregate can be trapped between coarser
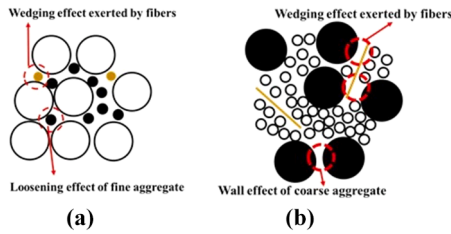
Fig. 7. Decreasing packing density of fiber-aggregate skeleton due to wedging effect in the mixtures, including (a) coarser and (b) finer particles.

ones and lead to more voids. This is referred to as the wedging effect (Fig. 5b).

On the other hand, when the content of finer particles is high, adding coarser aggregate may lead to create interparticle voids due to wall effect, which are not large enough to be filled with finer aggregate. This can result in lower packing density (Fig. 5b). In the case of F-A combination, fibers can be cross-sectionally and longitudinally placed between aggregate, as illustrated in Fig. 6a and 6b, respectively.

Accordingly, the packing density of F-A mixture can decrease due to the wedging effect of fibers' cross section, especially when incorporated at higher content than the optimum one, and loosening effect of finer aggregate (Fig. 7a). On the other hand, in the presence of finer aggregate (Fig. 7b), the packing density of F-A combination can decrease because of wedging effect of longitudinally oriented fibers and wall effect of coarser particles.

As can be observed in Fig. 4a and 4b, the incorporation of polyolefin synthetic fibers (IT and ST) reduced the LPD of the investigated F-A mixtures. It can be explained by the fact that addition of polyolefin fibers

beyond a certain content can increase the fiber-coarse aggregate interaction, thus leading to potential formation of fiber clumping. This can cause non-uniform fiber distribution throughout the F-A matrix, hence decreasing the LPD. On the other hand, increasing the PPF fiber content from 0.4% to 0.6% and 0.9% resulted in 1% increase and 2.1% decrease, respectively, in the LPD of F-A mixtures proportioned with MSA14-3 coarse aggregate mixture. It is worthy to mention that the accuracy of the PD measurements was evaluated using the coefficient of variation (COV$_{PD}$) of the PD values of three trial samples for each coarse aggregate mixture (Table 1) and F-A mixture (Figs. 3 and 4), as follows:

$$COV_{PD}\ (\%) = \frac{SD_{PD}}{AVG_{PD}} \times 100\% \tag{1}$$

where SD$_{PD}$ and AVG$_{PD}$ are the standard deviation and average of PD values of three samples for each coarse aggregate and F-A mixture, respectively. According to the carried-out error analyses, COV$_{PD}$ values of the investigated coarse aggregate mixtures (PD$_A$ values in Table 1) and F-A mixtures proportioned with macro-steel (Fig. 3a and 3c), micro-steel (Fig. 3b and 3d), ST (Fig. 4a), IT (Fig. 4b), PPF (Fig. 4c), PSI (Fig. 4d), and TUF (Fig. 4e) fibers ranged from 0 to 0.10%, 0 to 0.31%, 0 to 0.28%, 0.03% to 0.16%, 0 to 0.24%, 0.03% to 0.13%, 0 to 0.21%, and 0.03% to 0.10%, respectively. It can be concluded that measurement errors are negligible compared to the reported PD values (low COV$_{PD}$ values).

In loose state (i.e., without any compaction), adding fibers can change the arrangement of aggregate in F-A matrix depending on their size and volumetric content. Accordingly, the LPD of the coarse aggregate mixtures is compared to those incorporating different fiber contents. The PD of aggregate in F-A mixtures was evaluated, as follows:
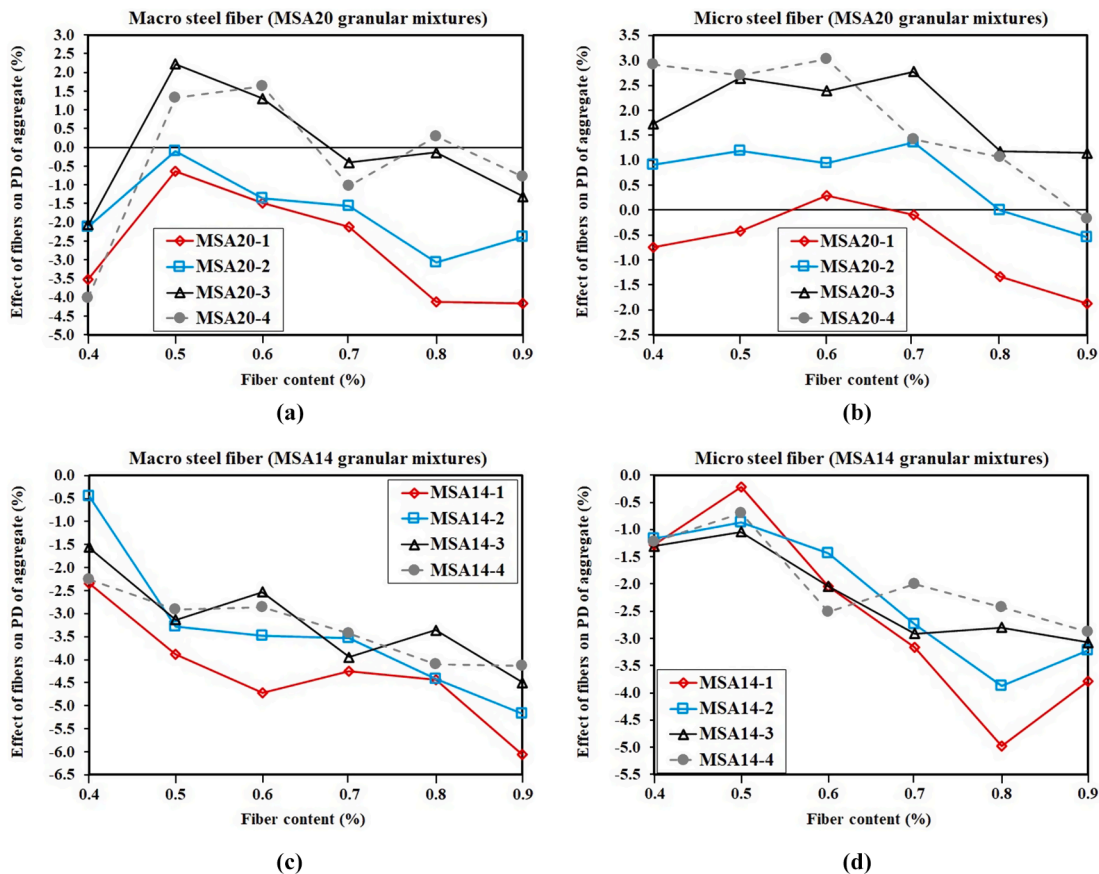

Fig. 8. Effect of fiber content on packing density of coarse aggregate in F-A mixtures proportioned with (a, b) MSA20 and (c, d) MSA14 coarse aggregate mixtures, as well as (a, c) macro and (b, d) micro steel fibers.
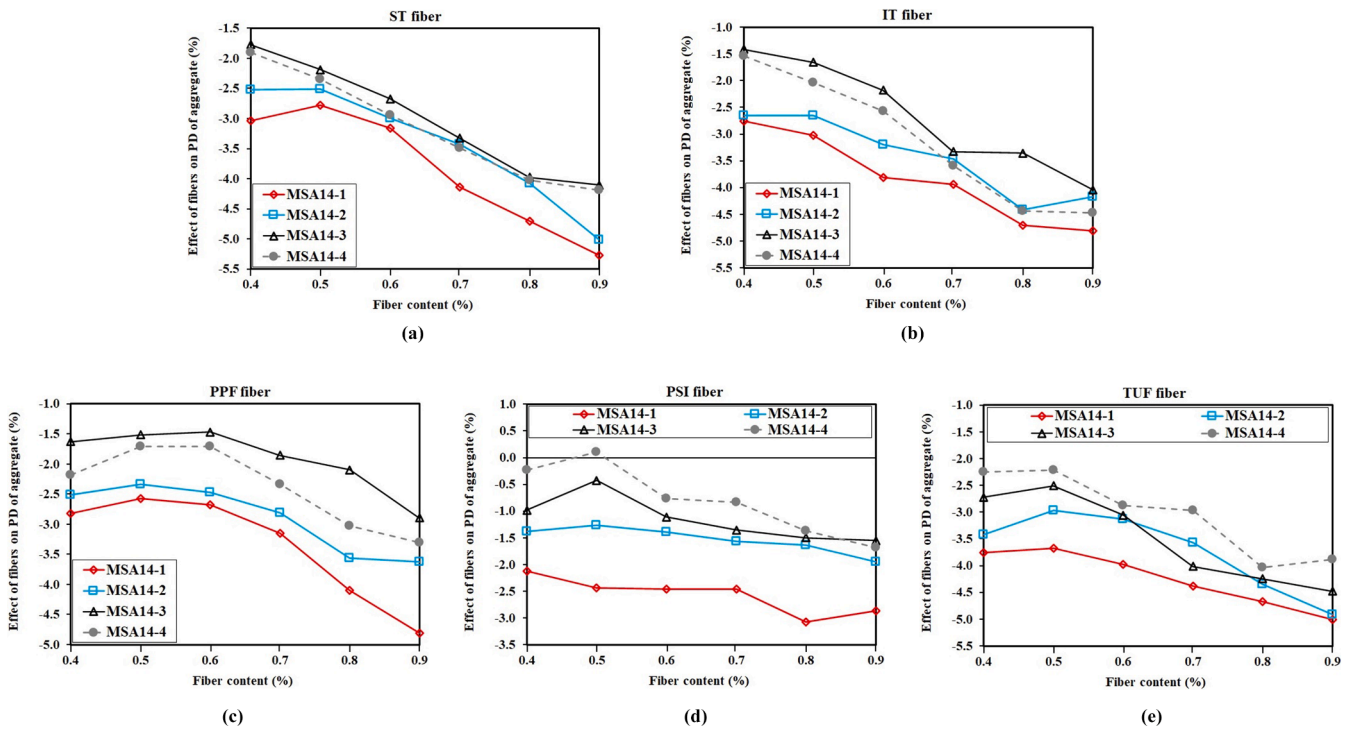
Fig. 9. Effect of fiber content on PD of coarse aggregate in F-A mixtures proportioned with MSA14 coarse aggregate mixtures and synthetic fibers, including (a) ST, (b) IT, (c) PPF, (d) PSI, and (e) TUF fibers.

Table 4
DPD of fibers obtained using ICT device.

Fiber type	Steel fibers		Polypropylene fibers		Polyolefin fibers		
	Macro	Micro	PPF	PSI	TUF	IT	ST
PD	0.065	0.068	0.106	0.204	0.081	0.064	0.076

$$\text{PD of aggregate in F-A mixture} = \frac{V_{Agg}}{V_{Total} = \pi \times r^2 \times h} \qquad (2)$$

where V_{Agg} and r correspond to the volume of coarse aggregate and radius of tested samples (50 mm), respectively, while h is the height of the sample at the end of PD measurements. The effect of fibers on PD of aggregate was then evaluated, as follows:

$$\text{Effect of fibers on PD of aggregate} = \frac{\text{PD of Agg in F-A mixture} - \text{PD}_{Agg}}{\text{PD}_{Agg}} \times 100\% \qquad (3)$$

where "PD_{Agg}" is the PD of the investigated coarse aggregate mixtures (Table 1) without any fibers (i.e., $V_f = 0$). The changes in PD of aggregate in F-A mixture, obtained using Eq. (3), are plotted against the volumetric contents of the steel and synthetic fibers in Figs. 8 and 9, respectively. As shown earlier, the COV_{PD} values of the PD_{Agg} measurements ranged from 0 to 0.10% which are negligible compared to the values reported in Figs. 8 and 9. Hence, this can confirm the validity of the evaluated results of fiber effect on PD of coarse aggregate, presented in Figs. 8 and 9.

As can be observed in Fig. 8, increasing the steel fiber content up to an optimum value can increase the PD of coarse aggregate in F-A mixtures relative to those of the coarse aggregate mixtures without fibers. However, adding higher fiber content than the optimum value negatively affects PD of coarse aggregate. This can be due to the wedging effect of fiber on packing density of coarse aggregate skeleton (Fig. 7). On the other hand, increasing synthetic fiber' content led to decrease in PD of coarse aggregate, as shown in Fig. 9.

As can be observed in Figs. 8 and 9, the incorporation of micro steel and PP fibers led to lower negative effect on PD of coarse aggregate compared to those obtained for F-A mixtures containing macro steel and polyolefin fibers. In order to explain this phenomenon, the DPD of different fibers were measured, using the ICT device and testing procedure explained earlier (i.e., under 50 gyratory cycles and 20 kPa normal pressure). As summarized in Table 4, the maximum DPD of fibers was found for PSI polypropylene fibers which also showed the higher LPD of F-A, as indicated in Fig. 4. Moreover, micro steel and PP fibers exhibited higher DPD values than macro steel and polyolefin ones, respectively. This suggests that micro steel and PP fibers can achieve higher level of compaction within the voids of a given PSD of aggregate compared to those obtained for the macro steel and polyolefin ones. It is also worth mentioning that relatively low DPD of fibers can be due to their rod shapes. It can be concluded that the packing density of F-A mixture is a function of both fibers and aggregate characteristics in terms of fiber content, type, and PD of fibers, as well as the mean diameter of interparticle voids which directly depends on the PSD of aggregate.

3.2. Effect of fiber size on LPD of the investigated F-A mixtures

As explained earlier, the LPD of F-A mixtures are dependent only on the size (length L_f and diameter D_f) of the fibers rather than their rigidity. This is reflected by non-deformed fibers after four gyratory-cycles compaction. In order to evaluate this effect, the LPD of the F-A mixtures containing relatively small and larger fibers were compared. Accordingly, for a given PSD of coarse aggregate mixture and fiber content, the LPD values obtained for the micro steel (L_f of 13 mm and D_f of 0.2 mm) and PPF fibers (L_f of 38 mm and D_f of 0.39 mm) were compared to those obtained with the macro steel (L_f of 30 mm and D_f of 0.55 mm) and TUF fibers (L_f of 38 mm and D_f of 0.69 mm), respectively, as shown in Fig. 10.

As can be observed in Fig. 10, for a given PSD of coarse aggregate, decreasing the fiber size (i.e., lower L_f and D_f) led to higher LPD of F-A mixtures. In loose state, the shorter and thinner fibers can properly fill the interparticle voids (Fig. 11a) and, therefore, increase the LPD of the

Table 5
Results of the robustness analyses carried out on the LPD of F-A mixtures.

| Model	Robustness analysis method	Variations of the effective parameters								Precision		Robustness analysis results	
		PD_A	D_f	L_f	V_f	D_A	E	I	$LPD_{F\text{-}A}$	RMSE	R^2	ΔRMSE	ΔR^2
LPD - Eq. (7)	1-way	±5%	–	–	–	–	–	–	–	0.0512–0.0537	0.0013–0.6933	0.048335–0.050850	(−0.8881) – (−0.1960)
		–	±5%	–	–	–	–	–	–	0.0028–0.0029	0.8891–0.8896	0.000005–0.000013	(−0.000268) – (0.000220)
		–	–	±5%	–	–	–	–	–	0.0027–0.0028	0.8893–0.8894	(−0.0000001) – (0.0000001)	(−0.0000055) – (0.0000052)
		–	–	–	±5%	–	–	–	–	0.00294–0.00295	0.8886–0.8898	0.000049–0.000067	(−0.00077) – (0.00041)
		–	–	–	–	±5%	–	–	–	0.0028–0.0029	0.8891–0.8896	0.000005–0.000014	(−0.000283) – 0.000211
	2-way	±5%	±5%	–	–	–	–	–	–	0.0510–0.0539	0.0006–0.6935	0.048132–0.051101	(−0.8888) – (−0.1959)
		±5%	–	±5%	–	–	–	–	–	0.0512–0.0537	0.0012–0.6933	0.048331–0.050855	(−0.8881) – (−0.1960)
		±5%	–	–	±5%	–	–	–	–	0.0507–0.0544	0.00005–0.6935	0.047824–0.051472	(−0.8893) – (−0.1959)
		±5%	–	–	–	±5%	–	–	–	0.0510–0.0540	0.0006–0.6935	0.048141–0.051089	(−0.8887) – (−0.1959)
		–	±5%	±5%	–	–	–	–	–	0.0028–0.0029	0.8891–0.8896	0.000005–0.000014	(−0.00027) – (0.00022)
		–	±5%	–	±5%	–	–	–	–	0.0029–0.0030	0.8882–0.8898	0.000017–0.000125	(−0.0012) – (0.00045)
		–	±5%	–	–	±5%	–	–	–	0.0028–0.0029	0.8887–0.8897	0–0.000046	(−0.0006) – (0.0004)
		–	–	±5%	±5%	–	–	–	–	0.0029–0.0030	0.8886–0.8898	0.000048–0.000068	(−0.00078) – (0.00041)
		–	–	±5%	–	±5%	–	–	–	0.0028–0.0029	0.8891–0.8896	0.000004–0.000015	(−0.00029) – (0.00021)
		–	–	–	±5%	±5%	–	–	–	0.0029–0.0030	0.8882–0.8898	0.000015–0.000128	(−0.0012) – (0.00045)
	3-way	±5%	±5%	±5%	–	–	–	–	–	0.0510–0.0540	0.00055–0.6935	0.048127–0.051106	(−0.8888) – (−0.1959)
		±5%	±5%	–	±5%	–	–	–	–	0.0515–0.0546	0.00002–0.6936	0.047625–0.051718	(−0.8893) – (−0.1958)
		±5%	±5%	–	–	±5%	–	–	–	0.0508–0.0542	0.0002–0.6936	0.047940–0.051338	(−0.8892) – (−0.1958)
		±5%	–	±5%	±5%	–	–	–	–	0.0507–0.0544	0.000043–0.6935	0.047820-0.051477	(−0.8893) – (−0.1959)
		±5%	–	±5%	–	±5%	–	–	–	0.0510–0.0540	0.0006–0.6935	0.048137–0.051094	(−0.8888) – (−0.1959)
		–	±5%	±5%	±5%	–	–	–	–	0.0029–0.0030	0.8882–0.8898	0.000016–0.000127	(−0.0012) – (0.0004)
		–	±5%	±5%	–	±5%	–	–	–	0.0028–0.0029	0.8887–0.8897	0–0.00005	(−0.0006) – (0.0004)
		–	–	±5%	±5%	±5%	–	–	–	0.0029–0.0030	0.8881–0.8898	0.000015–0.00013	(−0.0012) – (0.0004)
		–	±5%	–	±5%	±5%	–	–	–	0.0029–0.0031	0.8877–0.8898	0–0.0002	(0.0016) – (0.0004)
		±5%	–	–	±5%	±5%	–	–	–	0.0505–0.0546	0.000015–0.6936	0.047634–0.051706	(−0.8893) – (−0.1958)
	4-way	±5%	±5%	±5%	±5%	–	–	–	–	0.0505–0.0546	0.00002–0.6936	0.047621–0.051723	(−0.8893) – (−0.1958)
		±5%	±5%	±5%	–	±5%	–	–	–	0.0508–0.0542	0.00016–0.6936	0.047935–0.051343	(−0.8892) – (−0.1958)
		±5%	±5%	–	±5%	±5%	–	–	–	0.0503–0.0548	0.00005–0.6937	0.047437–0.051951	(−0.8893) – (−0.1957)
		±5%	–	±5%	±5%	±5%	–	–	–	0.0505–0.0546	0.000013–0.6936	0.047630–0.051711	(−0.8893) – (−0.1958)
		–	±5%	±5%	±5%	±5%	–	–	–	0.0029–0.0037	0.8240–0.8898	0–0.0008	(−0.0653) – (0.0004)
	5-way	±5%	±5%	±5%	±5%	±5%	–	–	–	0.0503–0.0548	0.00004–0.6937	0.047433–0.051956	(−0.8893) – (−0.1957)
DPD - Eq. (9)	1-way	–	–	–	–	–	±5%	–	–	0.0032–0.0033	0.9098–0.9099	−0.000011–0.000022	0.001
		–	–	–	–	–	–	±5%	–	0.0032–0.0033	0.9099–0.9100	−0.000005–0.000005	0.001
		–	–	–	–	–	–	–	±5%	0.0276–0.0277	0.9099–0.9100	0.024361–0.024470	0.001
	2-way	–	–	–	–	–	±5%	±5%	–	0.0032–0.0033	0.9098–0.9098	−0.000012–0.000031	0.0001
		–	–	–	–	–	±5%	–	±5%	0.0271–0.0282	0.9098–0.9099	0.024162–0.024651	0.0001
		–	–	–	–	–	–	±5%	±5%	0.0276–0.0278	0.9098–0.9098	0.024302–0.024523	0.0001
	3-way	–	–	–	–	–	±5%	±5%	±5%	0.0274–0.0280	0.9098–0.9098	0.024103–0.024704	0.0001
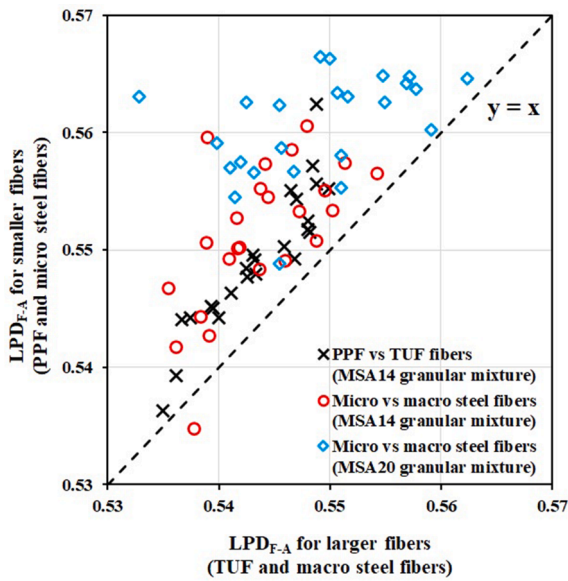
Fig. 10. Comparison between LPD of F-A mixtures made with given PSDs of coarse aggregate and fiber contents and different fibers' sizes (PPF, micro steel fibers, TUF, and macro steel fibers).
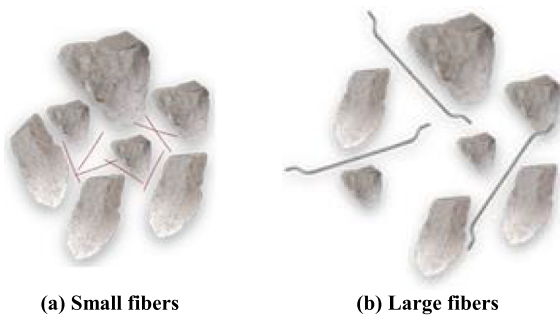

(a) Small fibers   **(b) Large fibers**

Fig. 11. Negative effect of increasing fiber size on LPD of F-A mixtures.
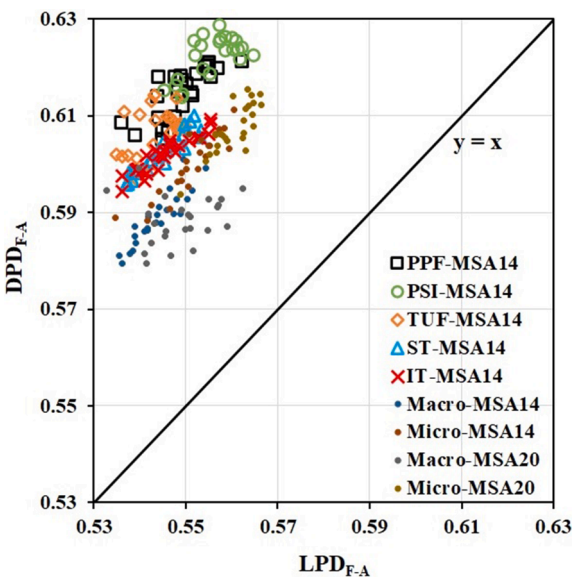

Fig. 12. Comparison between the DPD and LPD values of the investigated F-A mixtures.

F-A mixtures. However, the longer and thicker fibers can push away aggregate particles and lower the LPD of F-A mixture (Fig. 11b). For example, for a fiber volume of 0.5% and PSD of MSA20-4, increasing D_f and L_f of steel fibers from 0.20 to 0.55 mm and 13 to 30 mm decreased the LPD values of the F-A mixtures from 0.566 to 0.523, respectively.

3.3. Effect of fiber rigidity on DPD of the investigated F-A mixtures

In transition from the loosely- to densely-packed PD states, the compaction energy can lead to deform the fibers through the interparticle voids, depending on their rigidity. Therefore, the variation of PD of the investigated F-A mixtures from LPD to DPD state can reflect the effect of fibers' rigidity on PD of the F-A mixtures (Fig. 12), for a given PSD of coarse aggregate mixtures.

As expected, the DPD values of the F-A mixtures obtained after 50 gyratory cycles are higher than their corresponding LPD values after four gyratory cycles (Fig. 12). This is due to more deformation of the fibers under higher numbers of gyratory cycles, hence lowering the interparticle distances and increasing the PD. The deformation (y) of a single fiber located between two individual aggregate with an interparticle distance L_f (fiber length) and subjected to a compaction force F can be estimated, as shown in Fig. 13a and Eq. (4):

$$\text{Fiber deformation}: y \propto \frac{F \times L_f^3}{E \times I} \tag{4}$$

where E and I are the modulus of elasticity and second moment of area of fiber's cross section, respectively. Therefore, for a given PSD of aggregate (i.e., given apparent interparticle distance L_f) and given compaction energy (i.e., given F), the fiber deformation (y) depends mainly on the rigidity of the fibers, which can be characterized by $E \times I$. The variations of the DPD-to-LPD ratios of the investigated F-A mixtures with their corresponding fibers' rigidity indices ($E \times I$) are shown in Fig. 13b. The increase in fiber rigidity led to lower relative increase in DPD of the F-A mixtures compared to their corresponding LPD values. This is due to lower deformation of more rigid fibers under a given number of gyratory cycles. More specifically, F-A mixtures containing synthetic flexible fibers exhibited higher DPD-to-LPD ratios compared to those proportioned with rigid steel fibers. The maximum DPD-to-LPD ratio was obtained for the most flexible fibers of polypropylene PPF and TUF. As an illustrative example, the deformation of the micro- and macro-steel fibers are presented in Fig. 14a and 14b, respectively. The application of 50 gyratory cycles resulted in lower deformation of macro fibers (1.6 mm/13.4 mm = 12%) compared to that obtained for the micro fibers (1 mm/6.5 mm = 15%). This can be attributed to the higher relative rigidity of the macro fibers compared to the micro fibers.

3.4. Effect of PSD of coarse aggregate skeleton on LPD of the investigated F-A mixtures

In addition to fibers, LPD of F-A mixtures is influenced by aggregate characteristics. Adding a given content and type of fiber to fine and coarse PSD of aggregate can lead to opposite effects on PD of F-A mixtures. Adding fibers to a densely-packed granular mixture of finer PSD can push away the aggregate and decrease the LPD of F-A mixtures. On the other hand, in the case of a loosely-packed granular mixture of coarser PSD, fibers can fit easily in the large interparticle voids and increase the LPD of F-A mixtures.

In order to evaluate the effect of coarse aggregate on LPD of F-A mixtures, the investigated coarse aggregate mixtures were characterized in terms of their mean diameter (D_A) and mean 3D-surface area-to-volume ratio (AV_A) (Table 1). As shown in Fig. 15, the incorporation of a given fiber content of 0.5% to coarser granular mixtures (i.e., higher D_A) resulted in higher LPD of F-A mixtures.

On the other hand, the mean diameter of voids (D_v) was calculated as the ratio of voids' volume ($V_v = 1 - LPD_{F-A}$)-to-the 3D surface area of
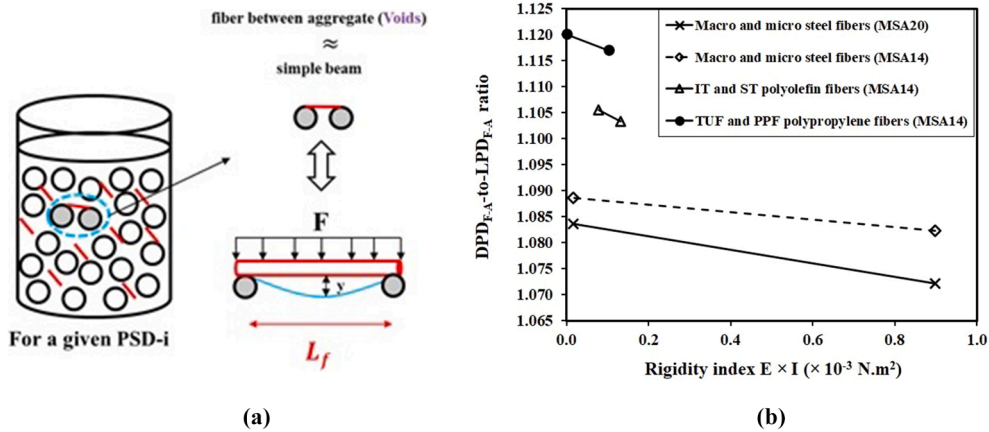
Fig. 13. (a) Fiber deformation between aggregate and (b) variation of the DPD-to-LPD ratios of the investigated F-A mixtures versus fibers' rigidity index (E × I).
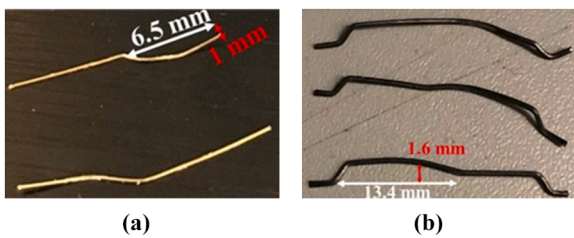
Fig. 14. Comparison between the deformations of (a) micro- and (b) macro-steel fibers under 50 gyratory cycles and given PSD of coarse aggregate mixture.
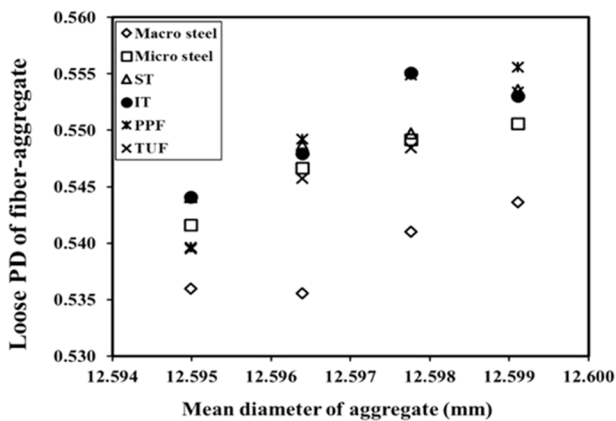
Fig. 15. Effect of mean diameter of coarse aggregate D_A on LPD of F-A mixtures.
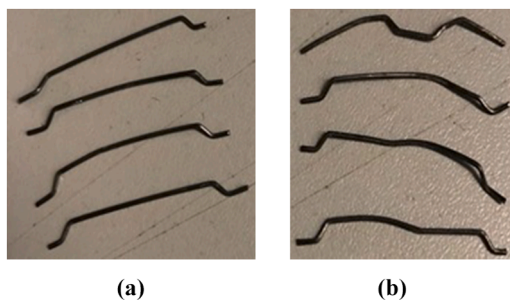
Fig. 16. Deformed fibers after DPD measurements of F-A mixtures proportioned with (a) MSA20-1 and (b) MSA20-2 coarse aggregate mixtures.

aggregate in unit volume of F-A (A_A), as follows:

$$D_v = \frac{V_v}{A_A} = \frac{1 - LPD_{F-A}}{V_A \times AV_A} = \frac{1 - LPD_{F-A}}{(LPD_{F-A} - V_f) \times AV_A} \tag{5}$$

where V_A and V_f are the volumetric contents of coarse aggregate and fibers in a unit volume of F-A mixture, respectively. The increase of D_v between aggregate particles leads to more available space for the fibers to be deformed under compaction, hence increasing the DPD of the F-A mixtures. As an example, illustrated in Fig. 16, the F-A mixtures proportioned with 0.6% and 0.9% of macro steel fiber and coarse aggregate mixtures MSA20-1 and MSA20-2 were compared. It is worthy to mention that without fiber, the coarse aggregate mixture MSA20-1 exhibited higher PD_A than MSA20-2 (Table 1). The fiber deformation after PD measurements was evaluated by the mean values of the ratio of the fiber deflections-to-the total fiber length (in %) using image analysis (Fig. 16). As can be observed in Figs. 16b and 17a, larger mean diameter of voids D_v, obtained for lower LPD, resulted in higher fiber deformations after PD measurements, hence increasing the DPD of F-A mixtures (Fig. 17b).

3.5. Coupled effect of fibre characteristics and coarse aggregate skeleton on PD of F-A mixtures

Given the above-mentioned observations, the coupled effect of characteristics of fibers, including volumetric content, size, and rigidity, as well as coarse aggregate skeleton, including average diameter and PD, on LPD and DPD of the investigated F-A mixtures are evaluated.

3.5.1. LPD model for F-A mixtures

As mentioned earlier (section 2.1), in order to investigate the LPD values, based on different PSD of coarse aggregates and fiber types and content, totally 160 F-A mixtures were prepared and tested. Then, as shown in Table A.1 in Appendix, 126 F-A mixtures were selected randomly out of 160 mixtures to establish the LPD model, and the rest (34 F-A mixtures) were used to validate this model (Table A.2 in Appendix). It is worth mentioning that each F-A mixture has been entitled by an ID including: application (R for repair and P for precast application)-fiber type-fiber volume (%)-MSA of coarse aggregate-PSD code. An empirical model was established to evaluate the coupled effect of volumetric content (V_f), length (L_f), and diameter (D_f) of the fibers and the average diameter (D_A) and PD of the coarse aggregate (PD_A) on the LPD of F-A mixtures. In order to establish such model, the following conditions must be fulfilled:

(i) if $V_f = 0 \rightarrow LPD_{F-A} = PD_A$
(ii) Based on Fig. 10: Higher $D_f \rightarrow$ Lower LPD_{F-A} values are expected
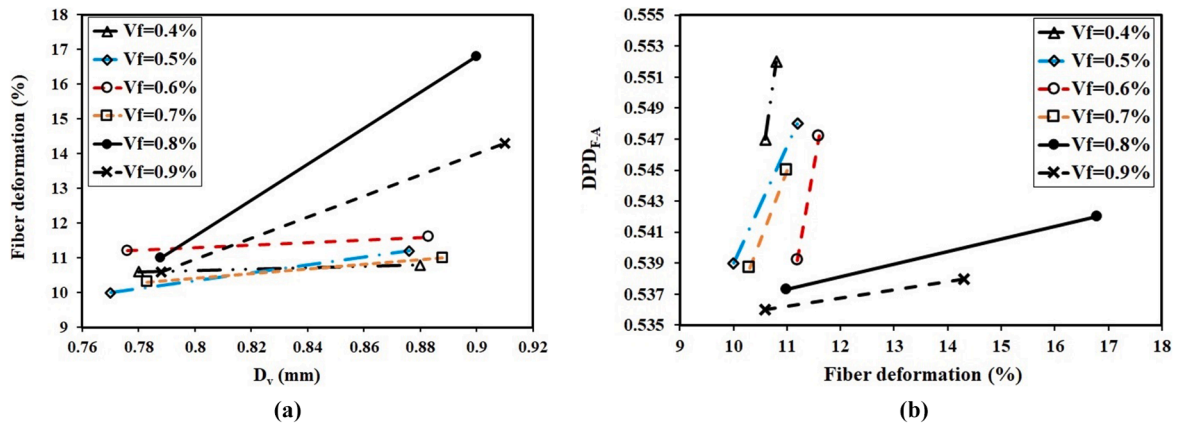
Fig. 17. Effect of (a) mean diameter of voids D_v on fiber deformation and (b) fiber deformation on DPD of F-A mixtures proportioned with 0.6% and 0.9% macro steel fibers and coarse aggregate mixtures MSA20-1 and MSA20-2.
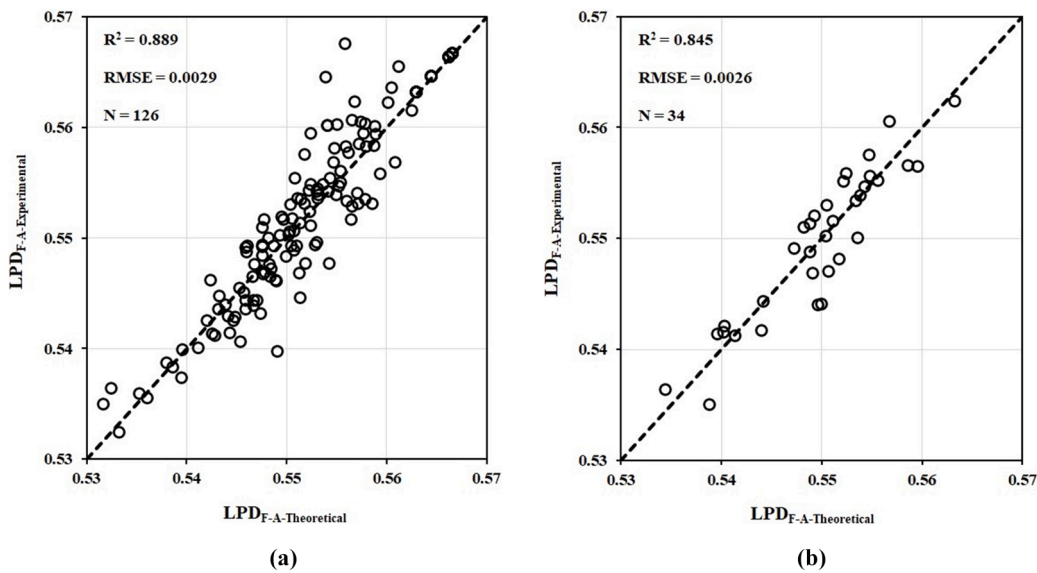
Fig. 18. (a) Comparison between the experimental and predicted LPD of the investigated F-A mixtures (Table A.1 in Appendix) and (b) validation of LPD model for F-A mixtures (Table A.2 in Appendix).

(iii) Based on Fig. 15: Higher $D_A \rightarrow$ Higher LPD_{F-A} values are expected

Since any direct positive or negative effect of PD of aggregate on LPD_{F-A} values was not observed, a polynomial contribution was considered for the PD_A values. This can lead to identify the optimum PD of coarse aggregate allowing higher LPD_{F-A} values. Regarding the first abovementioned condition (i), the contribution of PD_A values in the established model was assumed to be raised to the power of V_f contribution. A power law contribution was also considered for the V_f. Moreover, the effect of fibers on the LPD_{F-A} was taken into account by considering a product of power-law contributions of their content (V_f), diameter (D_f), and length (L_f) values, fulfilling the second

abovementioned condition (ii). Furthermore, a power law contribution of D_A was considered in the established model, referring to the third condition (iii). Accordingly, the following pattern was applied in a Microsoft Excel solver to evaluate the coupled effect of characteristics of fibers and aggregate on LPD_{F-A} values:

$$LPD_{F-A} = \frac{\left(A' \times PD_A^{B'} + C' \times PD_A + D'\right)^{\left(V_f^{E'}\right)} \times \left(1 - V_f^{F'}\right)}{1 + V_f^{G'} \times \left(\frac{D_f}{D_A}\right)^{H'} \times L_f^{I'}} \times PD_A^{\left(J' \, V_f\right)} \quad (6)$$

The following correlation was then established using the 126 selected F-A mixtures (Table A.1 in Appendix):

$$LPD_{F-A} = \frac{\left(1.9543 \times PD_A^{1.0812} - 0.0003 \times PD_A - 0.0170\right)^{\left(V_f^{0.0045}\right)} \times \left(1 - V_f^{146.4166}\right)}{1 + \frac{V_f^{0.4662} \times \left(\frac{D_f}{D_A}\right)^{0.1782}}{L_f^{0.0039}}} \times PD_A^{\left(0.8105 V_f\right)} \quad (7)$$
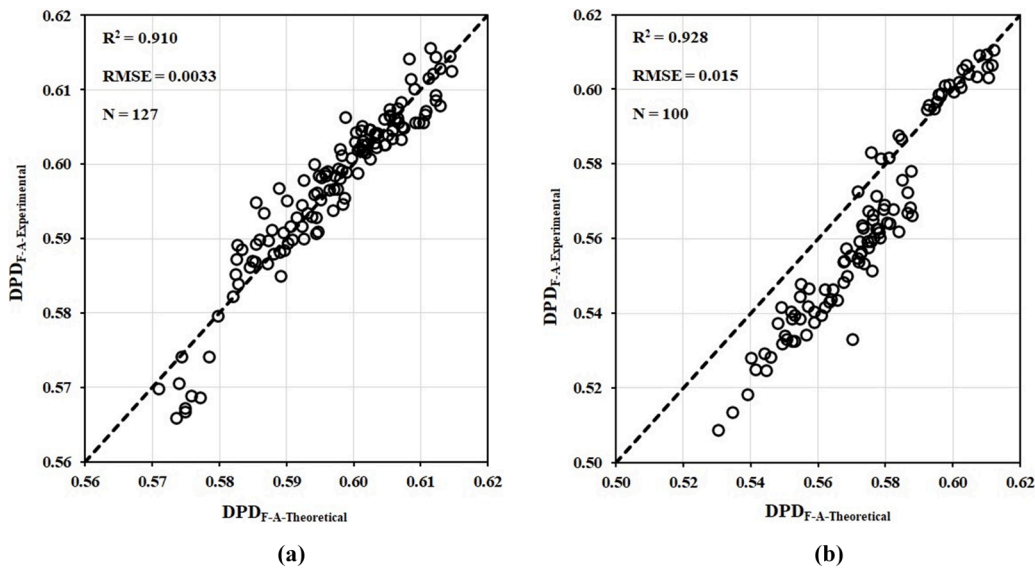
Fig. 19. (a) Comparison between experimental values of the DPD of the F-A mixtures (Table A.3 in Appendix) and those obtained using the empirical correlation (Eq. (9)) and (b) validation of the established DPD model (Eq. (9) to predict the DPD of F-A mixtures (Table A.4 in Appendix).
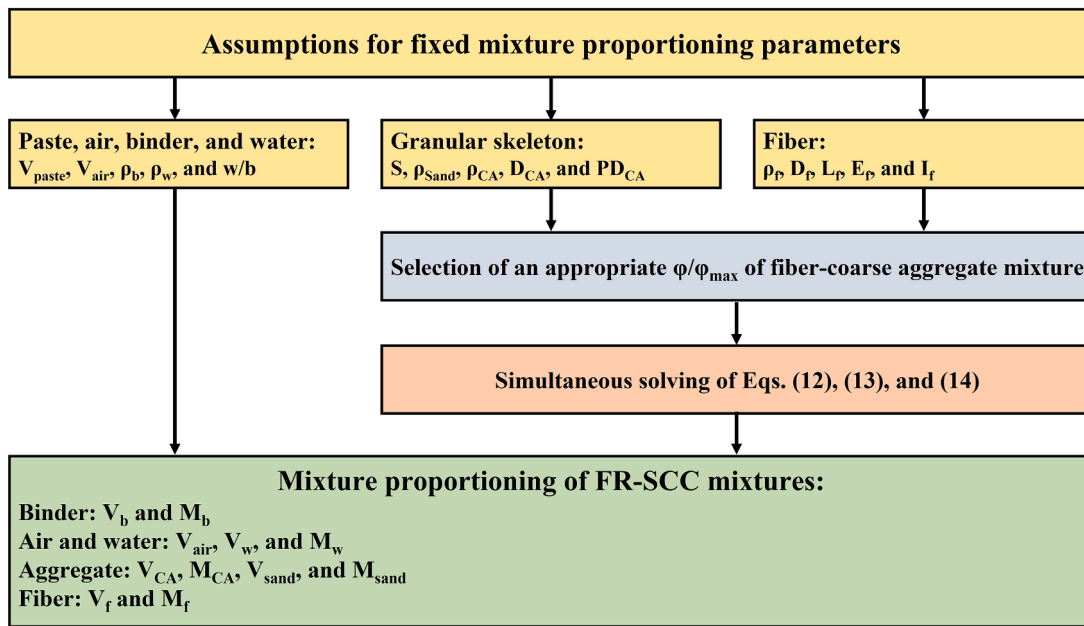
Fig. 20. Mixture proportioning approach of FR-SCC mixtures using the proposed models for the LPD and DPD of F-A combinations (Eqs. (7) and (9)).

It is worth noting that the established correlation covers a wide range of fiber contents (0.40%–1.77%) and types, including polypropylene (PPF and TUF), polyolefin (IT and ST), and steel (macro and micro) fibers of different sizes. This also includes a wide range of PSD of the coarse aggregate mixtures (Table 1). As shown in Fig. 18a, the experimental LPD values of the 126 selected F-A mixtures (Table 1.A in Appendix) were compared to those obtained using the empirical correlation given in Eq. (7). The accuracy of the established correlation was evaluated using the correlation coefficient (R^2) and the root-mean-square error (RMSE) defined in Eq. (8).

$$RMSE = \sqrt{\frac{\sum_{i=1}^{N} \left(LPD_{F-A-Experimental-i} - LPD_{F-A-Theoretical-i} \right)^2}{N}} \quad (8)$$

where N = 126 is the number of the investigated F-A mixtures to

establish the empirical correlation Eq. (7). As can be observed in Fig. 18a, the predicted LPD values are in good agreement with their corresponding experimental ones (high R^2 of 0.889 and low RMSE of 0.0029).

As shown in Fig. 18b, the established correlation given by Eq. (7) was validated using 34 additional F-A mixtures (Table 2.A in Appendix). The proposed loose PD model is shown to predict well the loose PD values of the F-A mixtures with high R^2 of 0.845 and low RMSE of 0.0026. According to the obtained adjustment factors (A′-J′) in Eq. (7), the PD of coarse aggregate (PD_A) and fiber content (V_f) showed the most dominant effects on LPD of F-A mixtures. Moreover, the effects of PD_A and V_f on LPD of F-A mixtures were found to be interdependent. Furthermore, among the size characteristics, diameter of fiber (D_f) and coarse aggregate (D_A) showed more significant effect than fiber length (L_f).

3.5.2. DPD model for F-A mixtures

As explained earlier, when the F-A mixture with a given LPD is compacted, the rigidity of fibers can negatively affect the DPD state. A Microsoft Excel solver was established to evaluate the effect of fiber rigidity on DPD of F-A mixtures (DPD$_{F-A}$) compared to their LPD$_{F-A}$ values. The following empirical model was established using 127 F-A mixtures which were randomly selected among 156 F-A mixtures made with 0.4%–1.77% fiber volume using rigid (macro and micro steel) and semi-rigid (IT and ST polyolefin) fibers, as well as eight different PSD coarse aggregate mixtures described in section 2.1 (Table A.3 in Appendix). The remained 29 F-A mixtures (out of 156) in addition to 71 F-A mixtures that were taken from two lateral sections of the investigated the L-Box and T-Box tests, were then used to validate the DPD model (Table A.4 in Appendix). It is worth mentioning that each F-A mixtures has been entitled by an ID including: application (R for repair and P for precast application)-volume of paste (%) of FR-SCC mixture-fiber type-fiber volume (%)-MSA of coarse aggregate-PSD code-the set-up where the sample has been extracted from (L for L-Box and T for T-Box)-sampling zone of each test (E for end and B for beginning of L-Box set-up, as well as U for tilt-up and D for tilt-down zones of T-Box set-up).

$$DPD_{F-A} = 1.0546 \times \frac{LPD_{F-A}^{0.9204}}{E^{0.0066} \times I^{0.0019}} \tag{9}$$

where E and I are in GPa and mm^4, respectively. As can be observed in Fig. 19a, the DPD$_{F-A}$ values predicted using the empirical correlation given in Eq. (9) (DPD$_{F-A-Theoretical}$) for the 127 F-A mixtures are in good agreement with their corresponding experimental values (DPD$_{F-A-Experimental}$), with high R^2 of 0.910 and low RMSE of 0.0033. According to the obtained adjustment power indices in Eq. (9), it can be concluded that the LPD of the F-A mixtures dominantly control their DPD, which is itself dependent on various characteristics of fibers and coarse aggregate (Eq. (7)). Moreover, the rigidity of fibers had a negative effect on the DPD of F-A mixtures, reflected by E and I. Furthermore, the modulus of elasticity of fibers E showed more dominant effect on the DPD of the F-A mixtures compared to their second moment of area of fibers' cross section I (adjustment power index 0.0066 vs 0.0019).

As explained earlier in Section 2.1, the established model defined in Eq. (9) was validated for 100 selected F-A mixtures (Table A.4 in Appendix). Accordingly, the experimental and predicted DPD values, obtained using empirical Eq. (9) for 100 F-A mixtures (Table A.4 in Appendix) are compared in Fig. 19b. The results indicated that the established model can successfully predict the DPD of the selected F-A mixtures with high R^2 of 0.928 and low RMSE of 0.015.

3.5.3. Robustness of LPD and DPD models to variations in the F-A mixture components

The robustness of LPD and DPD values to small variations of F-A mixture parameters, including the PD (PD$_A$) and mean diameter (D$_A$) of the coarse aggregate, as well as diameter (D$_f$), length (L$_f$), volume (V$_f$), and rigidity (E and I) of the fibers was investigated. Accordingly, a variation of ±5% was considered for the effective parameters of the LPD (Eq. (7)) and DPD (Eq. (9)) models.

In the case of LPD values, 1-, 2-, 3-, 4-, and 5-way robustness analyses, corresponding to single, double, triple, quadruple, and quintuple variations of the PD$_A$, D$_A$, D$_f$, L$_f$, and V$_f$ parameters, were applied. Using the established correlation Eq. (7), the LPDs of the F-A mixtures proportioned with fibers and coarse aggregate having characteristics with ±5% relative variations to those of the investigated F-A mixtures used to develop Eq. (7) were evaluated. On the other hand, in the case of DPD values, the single, double, and triple ±5% variations of LPD$_{F-A}$, E, and I parameters were considered. Accordingly, using the established Eq. (9), the DPDs of the F-A mixtures, considering ±5% variations of LPD$_{F-A}$, as well as E and I of fibers of the investigated mixtures, used to develop Eq. (9), were calculated. In order to evaluate the robustness of the PD values of F-A mixtures, the variations in the RMSE (ΔRMSE) and

coefficients of determination (ΔR^2) of the LPDs and DPDs of the F-A mixtures, due to single and multiple ±5% variations of the corresponding parameters, relative to those obtained for the investigated F-A mixtures, presented in Figs. 18a and 19a, were calculated as follow:

$$\Delta RMSE = RMSE_{with\ variations} - RMSE_{without\ variations} \tag{10}$$

$$\Delta R^2 = R^2_{with\ variations} - R^2_{without\ variations} \tag{11}$$

where RMSE$_{without\ variations}$ (0.0029 and 0.0033) and R$^2_{without\ variations}$ (0.889 and 0.910) are the RMSE and R^2 values obtained for the LPD and DPD values using Eqs. (7) and (9) and presented in Figs. 18a and 19a, respectively. The results of the robustness analyses of the LPD and DPD values are summarized in Table 5.

As indicated in Table 5, the LPD of F-A showed its maximum robustness due to any single, double, triple, and quadruple ±5% variations of volume, length, and diameter of fibers, as well as mean diameter of coarse aggregate. This was reflected by low |ΔRMSE| and |ΔR^2| values up to 0.0008 and 0.0653, respectively. On the other hand, the most sensitivity of the LPD values of F-R mixtures were observed due to any single and multiple ±5% variations of PD of coarse aggregate skeleton, reflected by increasing RMSE up to higher 0.051956 values and decreasing R^2 values up to lower 0.8893 values.

As can be observed in Table 5, the DPD values of F-A mixtures showed their maximum robustness due to rigidity of fibers, reflected by any single and double ±5% variations in E and I of fibers (low |ΔRMSE| and |ΔR^2| values up to 0.000031 and 0.0001, respectively). However, the most sensitivity of the DPD values were observed for any ±5% variations of LPD of the F-A mixtures, reflected by high ΔRMSE values up to 0.024704.

4. New workability design for FR-SCC mixtures based on the established PD models of F-A combinations

Koura et al. [32] proposed a mixture proportioning approach for SCC as a diphasic suspension of coarse aggregate (>1.25 mm) and mortar with solid particles <1.25 mm. The authors reported that in addition to the rheological properties of fine mortar, the flowability [32], passing ability [12,32], and stability [11,13], as well as compressive strength of the SCC [32] are significantly influenced by the relative-solid packing fraction of coarse aggregate. This is defined as the ratio of the volumetric content (φ)-to-PD of coarse aggregate (φ/φ$_{max}$) in unit volume of SCC. The authors established empirical models to predict the flow and mechanical performance of SCC as a function of rheological properties of fine mortar and φ/φ$_{max}$ of coarse aggregate [11–13,32]. For a given volume and workability of mortar, the selection of an appropriate φ/φ$_{max}$ of coarse aggregate can lead to achieving the targeted workability characteristics and mechanical performance [32]. A similar approach can be employed to proportion FR-SCC as a diphasic suspension of suspending mortar (≤5 mm) and suspended fiber-coarse aggregate (F-A) mixtures (A > 5 mm). The following mixtures parameters are essential in designing FR-SCC: water-to-binder ratio (w/b), volume of paste (V$_{paste}$), air content (V$_{air}$), volumetric sand-to-total aggregate ratio (S), densities of fiber (ρ$_f$), binder (ρ$_b$), water (ρ$_w$), coarse aggregate (ρ$_{CA}$), and sand (ρ$_{sand}$), as well as the fiber length (L$_f$), fiber diameter (D$_f$), second moment of area of cross section of the fiber (I$_f$), and modulus of elasticity (E$_f$) of the fiber, as well as the mean-diameter (D$_{CA}$) and packing density (PD$_{CA}$) of coarse aggregate.

First, knowing the w/b, V$_{paste}$, V$_{air}$, ρ$_b$, and ρ$_w$ parameters, the required volumetric contents and masses of binder (V$_b$ and M$_b$) and water (V$_w$ and M$_w$) can be calculated. The volumes of sand (V$_{sand}$), coarse aggregate (V$_{CA}$), and fiber (V$_f$) can then be calculated, as follows:

$$V_{sand} + V_{CA} + V_f = 1 - (V_b + V_w + V_{air}) \tag{12}$$

By knowing S, the following relationship can be established between the V$_{sand}$ and V$_{CA}$:

$$\frac{V_{sand}}{V_{sand} + V_{CA}} = S \tag{13}$$

On the other hand, according to the empirical models and guidelines proposed by Hosseinpoor et al. [11,12] and Koura et al. [13,32], an appropriate volumetric content-to-PD ratio φ/φ_{max} of fiber-coarse aggregate combination is selected to achieve given workability and compressive strength values. Moreover, the PD of fiber-coarse aggregate combination φ_{max} can be evaluated using the proposed LPD and DPD models in this study (Eqs. (7) and (9)). Therefore, the following relationship can be established between V_{CA}, V_f, and characteristics of fiber and coarse aggregate:

$$\frac{(V_{CA} + V_f) \times E_f^{0.0066} \times I_f^{0.0019}}{1.0546 \times \left[\frac{(1.9543 \times PD_{CA}^{1.0812} - 0.0003 \times PD_{CA} - 0.0170)\left(\left(\frac{V_f}{V_f+V_{CA}}\right)^{0.0045}\right) \times \left(1 - \left(\frac{V_f}{V_f+V_{CA}}\right)^{146.4166}\right)}{1 + \frac{\left(\frac{V_f}{V_f+V_{CA}}\right)^{0.4662} \times \left(\frac{D_f}{D_{CA}}\right)^{0.1782}}{L_f^{0.0039}}} \times PD_{CA}^{\left(0.8105\left(\frac{V_f}{V_f+V_{CA}}\right)\right)}\right]^{0.9204}} = \frac{\varphi}{\varphi_{max}} \tag{14}$$

Eqs. (12), (13), and (14) are then simultaneously solved to calculate the volumetric contents of coarse aggregate (V_{CA}), sand (V_{sand}), and fiber (V_f). Their corresponding masses M_{CA}, M_{sand}, and M_f can also be calculated knowing the densities. A schematic flowchart of the proposed mixture proportioning approach of FR-SCC mixtures is presented in Fig. 20.

5. Conclusions

Understanding the coupled effect of fibers and coarse aggregate characteristics on packing density of F-A system in different compaction conditions can lead to better optimization of the performance of FRC SCC, in terms of workability and mechanical properties. In fact, enhancing the packing density of the solid skeleton, including fiber and aggregate, in FRC matrix can result in lowering the paste content for a given workability or increasing workability for a given paste content. In this study, the packing density of various fiber-coarse aggregate mixtures, under loosely- and densely-packed conditions, were investigated. Different levels of compaction was considered to simulate different packing condition during mixing and casting processes of FRC. Different types of fibers used at various volumetric contents, sizes, and rigidities, as well as different particle-size distributions of coarse aggregate were evaluated. Based on the experimental results reported in this study, two empirical models were proposed to predict the packing density of F-A mixtures in loose and compacted conditions. The following conclusions can be established from this study:

- The loosely-packed PD (LPD) of F-A mixtures was found to be mostly affected by the volumetric content and size of the fibers, as well as the mean diameter and PD of the coarse aggregate.
- For a given PSD of coarse aggregate, the incorporation of steel and polypropylene fibers up to an optimum value resulted in higher LPD of F-A mixtures beyond which the LPD decreased. This was found more significant for F-A mixtures proportioned with coarser PSD of granular skeleton and larger fibers. However, the incorporation of any volume of polyolefin fibers led to lower PD of aggregate compared to those obtained without any fiber.
- For a given PSD of coarse aggregate and fiber content, the incorporation of larger fibers resulted in lower LPD of the F-A mixtures. On the other hand, the incorporation of a given fiber volume to coarser PSD of coarse aggregate resulted in higher LPD of F-A mixtures.

- The densely-packed PD (DPD) of F-A mixtures were found to be more controlled by their PD in loosen state (LPD) and rigidity of the fibers. The F-A mixtures proportioned with more flexible fibers experienced higher DPD-to-LPD ratio comparing to the rigid fibers due to their higher deformation through the interparticle voids.
- Two new empirical models were proposed to predict the LPD and DPD of F-A mixtures as a function of the characteristics of the fibers and coarse aggregate skeleton. The LPD of the F-A mixtures were found in good correlations with volumetric content, length, and diameter of fibers, as well as the mean diameter and PD of coarse aggregate. The DPD of F-A mixtures were well correlated with modulus of elasticity and second moment of area of cross section of fibers, as well as their LPD values.
- Robustness analyses revealed that the LPD of F-A is quite sensitive to any variation of PD of the coarse aggregate skeleton which is directly dependent of PSD of coarse aggregate. However, the LPD values of F-A mixtures showed maximum robustness due to any single and multiple variations of volumetric content and size of fibers, as well as mean diameter of coarse aggregate. On the other hand, the DPD values of the F-A mixtures were found to be quite robust and highly sensitive to the variation of rigidity of fibers and their LPD values, respectively.
- A new workability-design approach was proposed for FR-SCC mixtures based on the established LPD and DPD models.

CRediT authorship contribution statement

Naimeh Nouri: Conceptualization, Methodology, Software, Validation, Formal analysis, Investigation, Data curation, Writing – review & editing, Writing – original draft, Supervision, Project administration. **Masoud Hosseinpoor:** Conceptualization, Methodology, Software, Validation, Formal analysis, Investigation, Resources, Data curation, Writing – review & editing, Writing – original draft, Supervision, Project administration. **Ammar Yahia:** Conceptualization, Methodology, Formal analysis, Investigation, Data curation, Writing – review & editing, Writing – original draft, Supervision, Project administration. **Kamal H. Khayat:** Conceptualization, Methodology, Formal analysis, Investigation, Data curation, Writing – review & editing, Writing – original draft, Supervision, Project administration.

Declaration of Competing Interest

The authors declare that they have no known competing financial interests or personal relationships that could have appeared to influence the work reported in this paper.

Application in Concrete Infrastructures, held by Professor Ammar Yahia of the Université de Sherbrooke.

Appendix

See

Table A1
Proportioning and characteristics of F-A mixtures selected to establish LPD model.

Mix. No.	F-A mixture ID	PSD of coarse aggregate	Fiber type	V_f (m³/m³)
1	R-0-14-1	MSA-14-1	No fiber	0
2	R-0-14-2	MSA-14-2		
3	R-0-14-3	MSA-14-3		
4	R-0-14-4	MSA-14-4		
5	R-MaS-0.4-14-1	MSA-14-1	Macro steel	0.004
6	R-MaS-0.4-14-2	MSA-14-2		0.004
7	R-MaS-0.4-14-3	MSA-14-3		0.004
8	R-MaS-0.5-14-2	MSA-14-2		0.005
9	R-MaS-0.5-14-3	MSA-14-3		0.005
10	R-MaS-0.5-14-4	MSA-14-4		0.005
11	R-MaS-0.6-14-1	MSA-14-1		0.006
12	R-MaS-0.6-14-2	MSA-14-2		0.006
13	R-MaS-0.6-14-3	MSA-14-3		0.006
14	R-MaS-0.6-14-4	MSA-14-4		0.006
15	R-MaS-0.7-14-1	MSA-14-1		0.007
16	R-MaS-0.7-14-3	MSA-14-3		0.007
17	R-MaS-0.7-14-4	MSA-14-4		0.007
18	R-MaS-0.8-14-1	MSA-14-1		0.008
19	R-MaS-0.8-14-2	MSA-14-2		0.008
20	R-MaS-0.8-14-4	MSA-14-4		0.008
21	R-MaS-0.9-14-1	MSA-14-1		0.009
22	R-MaS-0.9-14-2	MSA-14-2		0.009
23	R-MaS-0.9-14-3	MSA-14-3		0.009
24	R-MaS-1.62-14-1	MSA-14-1		0.0162
25	R-MaS-1.62-14-2	MSA-14-2		0.0162
26	R-MaS-1.62-14-3	MSA-14-3		0.0162
27	R-MaS-1.69-14-1	MSA-14-1		0.0169
28	R-MaS-1.69-14-2	MSA-14-2		0.0169
29	R-MaS-1.69-14-4	MSA-14-4		0.0169
30	R-MaS-1.77-14-1	MSA-14-1		0.0177
31	R-MaS-1.77-14-3	MSA-14-3		0.0177
32	R-MaS-1.77-14-4	MSA-14-4		0.0177
33	R-MiS-0.4-14-1	MSA-14-1	Micro steel	0.004
34	R-MiS-0.4-14-2	MSA-14-2		0.004
35	R-MiS-0.4-14-3	MSA-14-3		0.004
36	R-MiS-0.5-14-1	MSA-14-1		0.005
37	R-MiS-0.5-14-2	MSA-14-2		0.005
38	R-MiS-0.5-14-3	MSA-14-3		0.005
39	R-MiS-0.5-14-4	MSA-14-4		0.005
40	R-MiS-0.6-14-2	MSA-14-2		0.006
41	R-MiS-0.6-14-3	MSA-14-3		0.006
42	R-MiS-0.6-14-4	MSA-14-4		0.006
43	R-MiS-0.7-14-1	MSA-14-1		0.007
44	R-MiS-0.7-14-3	MSA-14-3		0.007
45	R-MiS-0.7-14-4	MSA-14-4		0.007
46	R-MiS-0.8-14-1	MSA-14-1		0.008
47	R-MiS-0.8-14-2	MSA-14-2		0.008
48	R-MiS-0.8-14-4	MSA-14-4		0.008
49	R-MiS-0.9-14-1	MSA-14-1		0.009
50	R-MiS-0.9-14-2	MSA-14-2		0.009
51	R-MiS-0.9-14-3	MSA-14-3		0.009
Mix. No.	F-A mixture ID	PSD of coarse aggregate	Fiber type	V_f (m³/m³)
52	R-ST-0.4-14-1	MSA-14-1	ST	0.004
53	R-ST-0.4-14-2	MSA-14-2		0.004
54	R-ST-0.4-14-3	MSA-14-3		0.004
55	R-ST-0.4-14-4	MSA-14-4		0.004
56	R-ST-0.5-14-2	MSA-14-2		0.005
57	R-ST-0.5-14-3	MSA-14-3		0.005
58	R-ST-0.5-14-4	MSA-14-4		0.005
59	R-ST-0.6-14-1	MSA-14-1		0.006
60	R-ST-0.6-14-3	MSA-14-3		0.006
61	R-ST-0.6-14-4	MSA-14-4		0.006
62	R-ST-0.7-14-1	MSA-14-1		0.007
63	R-ST-0.7-14-2	MSA-14-2		0.007
64	R-ST-0.7-14-4	MSA-14-4		0.007

Table A1 (*continued*)

Mix. No.	F-A mixture ID	PSD of coarse aggregate	Fiber type	V_f (m^3/m^3)
65	R-ST-0.8-14-1	MSA-14-1		0.008
66	R-ST-0.8-14-2	MSA-14-2		0.008
67	R-ST-0.8-14-3	MSA-14-3		0.008
68	R-ST-0.9-14-2	MSA-14-2		0.009
69	R-ST-0.9-14-3	MSA-14-3		0.009
70	R-ST-0.9-14-4	MSA-14-4		0.009
71	R-IT-0.4-14-1	MSA-14-1	IT	0.004
72	R-IT-0.4-14-2	MSA-14-2		0.004
73	R-IT-0.4-14-4	MSA-14-4		0.004
74	R-IT-0.5-14-1	MSA-14-1		0.005
75	R-IT-0.5-14-3	MSA-14-3		0.005
76	R-IT-0.5-14-4	MSA-14-4		0.005
77	R-IT-0.6-14-1	MSA-14-1		0.006
78	R-IT-0.6-14-2	MSA-14-2		0.006
79	R-IT-0.6-14-3	MSA-14-3		0.006
80	R-IT-0.7-14-1	MSA-14-1		0.007
81	R-IT-0.7-14-2	MSA-14-2		0.007
82	R-IT-0.7-14-3	MSA-14-3		0.007
83	R-IT-0.7-14-4	MSA-14-4		0.007
84	R-IT-0.8-14-3	MSA-14-3		0.008
85	R-IT-0.8-14-4	MSA-14-4		0.008
86	R-IT-0.9-14-2	MSA-14-2		0.009
87	R-IT-0.9-14-3	MSA-14-3		0.009
88	R-IT-0.9-14-4	MSA-14-4		0.009
89	R-PPF-0.4-14-2	MSA-14-2	PPF	0.004
90	R-PPF-0.4-14-3	MSA-14-3		0.004
91	R-PPF-0.4-14-4	MSA-14-4		0.004
92	R-PPF-0.5-14-1	MSA-14-1		0.005
93	R-PPF-0.5-14-3	MSA-14-3		0.005
94	R-PPF-0.6-14-1	MSA-14-1		0.006
95	R-PPF-0.6-14-2	MSA-14-2		0.006
96	R-PPF-0.6-14-3	MSA-14-3		0.006
97	R-PPF-0.6-14-4	MSA-14-4		0.006
98	R-PPF-0.7-14-1	MSA-14-1		0.007
99	R-PPF-0.7-14-2	MSA-14-2		0.007
100	R-PPF-0.8-14-3	MSA-14-3		0.007
101	R-PPF-0.8-14-1	MSA-14-1		0.008
102	R-PPF-0.8-14-2	MSA-14-2		0.008
103	R-PPF-0.8-14-3	MSA-14-3		0.008
104	R-PPF-0.8-14-4	MSA-14-4		0.008
105	R-PPF-0.9-14-1	MSA-14-1		0.009
106	R-PPF-0.9-14-3	MSA-14-3		0.009
107	R-PPF-0.9-14-4	MSA-14-4		0.009
Mix. No.	F-A mixture ID	PSD of coarse aggregate	Fiber type	V_f (m^3/m^3)
108	R-TUF-0.4-14-1	MSA-14-1	TUF	0.004
109	R-TUF-0.4-14-2	MSA-14-2		0.004
110	R-TUF-0.4-14-3	MSA-14-3		0.004
111	R-TUF-0.4-14-4	MSA-14-4		0.004
112	R-TUF-0.5-14-1	MSA-14-1		0.005
113	R-TUF-0.5-14-3	MSA-14-3		0.005
114	R-TUF-0.5-14-4	MSA-14-4		0.005
115	R-TUF-0.6-14-1	MSA-14-1		0.006
116	R-TUF-0.6-14-2	MSA-14-2		0.006
117	R-TUF-0.6-14-3	MSA-14-3		0.006
118	R-TUF-0.7-14-1	MSA-14-1		0.007
119	R-TUF-0.7-14-2	MSA-14-2		0.007
120	R-TUF-0.7-14-4	MSA-14-4		0.007
121	R-TUF-0.8-14-1	MSA-14-1		0.008
122	R-TUF-0.8-14-2	MSA-14-2		0.008
123	R-TUF-0.8-14-4	MSA-14-4		0.008
124	R-TUF-0.9-14-1	MSA-14-1		0.009
125	R-TUF-0.9-14-3	MSA-14-3		0.009
126	R-TUF-0.8-14-4	MSA-14-4		0.009

Table A2

Proportioning and characteristics of F-A mixtures selected to validate the established LPD model.

Mix. No.	F-A mixture ID	PSD of coarse aggregate	Fiber type	V_f (m³/m³)
1	R-MaS-0.4-14-4	MSA-14-4	Macro steel	0.004
2	R-MaS-0.5-14-1	MSA-14-1		0.005
3	R-MaS-0.7-14-2	MSA-14-2		0.007
4	R-MaS-0.8-14-3	MSA-14-3		0.008
5	R-MaS-0.9-14-4	MSA-14-4		0.009
6	R-MaS-1.62-14-4	MSA-14-4		0.0162
7	R-MaS-1.69-14-3	MSA-14-3		0.0169
8	R-MaS-1.77-14-2	MSA-14-2		0.0177
9	R-MiS-0.4-14-4	MSA-14-4	Micro steel	0.004
10	R-MiS-0.6-14-1	MSA-14-1		0.006
11	R-MiS-0.7-14-2	MSA-14-2		0.007
12	R-MiS-0.8-14-3	MSA-14-3		0.008
13	R-MiS-0.9-14-4	MSA-14-4		0.009
14	R-ST-0.5-14-1	MSA-14-1	ST	0.005
15	R-ST-0.6-14-2	MSA-14-2		0.006
16	R-ST-0.7-14-3	MSA-14-3		0.007
17	R-ST-0.8-14-4	MSA-14-4		0.008
18	R-ST-0.9-14-1	MSA-14-1		0.009
19	R-IT-0.4-14-3	MSA-14-3	IT	0.004
20	R-IT-0.5-14-2	MSA-14-2		0.005
21	R-IT-0.6-14-4	MSA-14-4		0.006
22	R-IT-0.7-14-1	MSA-14-1		0.007
23	R-IT-0.8-14-2	MSA-14-2		0.008
24	R-IT-0.9-14-1	MSA-14-1		0.009
25	R-PPF-0.4-14-1	MSA-14-1	PPF	0.004
26	R-PPF-0.5-14-2	MSA-14-2		0.005
27	R-PPF-0.6-14-4	MSA-14-4		0.006
28	R-PPF-0.7-14-4	MSA-14-4		0.007
29	R-PPF-0.9-14-2	MSA-14-2		0.009
30	R-TUF-0.5-14-2	MSA-14-2	TUF	0.005
31	R-TUF-0.6-14-4	MSA-14-4		0.006
32	R-TUF-0.7-14-3	MSA-14-3		0.007
33	R-TUF-0.8-14-3	MSA-14-3		0.008
34	R-TUF-0.9-14-2	MSA-14-2		0.009

Table A3

Proportioning and characteristics of F-A mixtures selected to establish DPD model (Eq. (9)).

Mix. No.	F-A mixture ID	PSD of coarse aggregate	Fiber type	V_f (m³/m³)
1	R-MaS-0.4-14-1	MSA-14-1	Macro steel	0.004
2	R-MaS-0.4-14-2	MSA-14-2		0.004
3	R-MaS-0.4-14-3	MSA-14-3		0.004
4	R-MaS-0.5-14-1	MSA-14-1		0.005
5	R-MaS-0.5-14-2	MSA-14-2		0.005
6	R-MaS-0.5-14-3	MSA-14-3		0.005
7	R-MaS-0.5-14-4	MSA-14-4		0.005
8	R-MaS-0.6-14-2	MSA-14-2		0.006
9	R-MaS-0.6-14-3	MSA-14-3		0.006
10	R-MaS-0.6-14-4	MSA-14-4		0.006
11	R-MaS-0.7-14-1	MSA-14-1		0.007
12	R-MaS-0.7-14-2	MSA-14-2		0.007
13	R-MaS-0.7-14-3	MSA-14-3		0.007
14	R-MaS-0.7-14-4	MSA-14-4		0.007
15	R-MaS-0.8-14-2	MSA-14-2		0.008
16	R-MaS-0.8-14-3	MSA-14-3		0.008
17	R-MaS-0.8-14-4	MSA-14-4		0.008
18	R-MaS-0.9-14-1	MSA-14-1		0.009
19	R-MaS-0.9-14-3	MSA-14-3		0.009
20	R-MaS-0.9-14-4	MSA-14-4		0.009
21	R-MaS-1.62-14-1	MSA-14-1		0.0162

Table A3 (*continued*)

Mix. No.	F-A mixture ID	PSD of coarse aggregate	Fiber type	V_f (m³/m³)
22	R-MaS-1.62-14-2	MSA-14-2		0.0162
23	R-MaS-1.62-14-3	MSA-14-3		0.0162
24	R-MaS-1.69-14-1	MSA-14-1		0.0169
25	R-MaS-1.69-14-2	MSA-14-2		0.0169
26	R-MaS-1.69-14-3	MSA-14-3		0.0169
27	R-MaS-1.69-14-4	MSA-14-4		0.0169
28	R-MaS-1.77-14-2	MSA-14-2		0.0177
29	R-MaS-1.77-14-3	MSA-14-3		0.0177
30	P-MaS-0.4-20-1	MSA-20-1		0.004
31	P-MaS-0.4-20-2	MSA-20-2		0.004
32	P-MaS-0.4-20-3	MSA-20-3		0.004
33	P-MaS-0.5-20-1	MSA-20-1		0.005
34	P-MaS-0.5-20-2	MSA-20-2		0.005
35	P-MaS-0.5-20-3	MSA-20-3		0.005
36	P-MaS-0.5-20-4	MSA-20-4		0.005
37	P-MaS-0.6-20-1	MSA-20-1		0.006
38	P-MaS-0.6-20-2	MSA-20-2		0.006
39	P-MaS-0.6-20-3	MSA-20-3		0.006
40	P-MaS-0.6-20-4	MSA-20-4		0.006
41	P-MaS-0.7-20-1	MSA-20-1		0.007
42	P-MaS-0.7-20-3	MSA-20-3		0.007
43	P-MaS-0.7-20-4	MSA-20-4		0.007
44	P-MaS-0.8-20-2	MSA-20-2		0.008
45	P-MaS-0.8-20-3	MSA-20-3		0.008
46	P-MaS-0.8-20-4	MSA-20-4		0.008
47	P-MaS-0.9-20-1	MSA-20-1		0.009
48	P-MaS-0.9-20-2	MSA-20-2		0.009
49	P-MaS-0.9-20-3	MSA-20-3		0.009
50	P-MaS-0.9-20-4	MSA-20-4		0.009
51	R-ST-0.4-14-2	MSA-14-2	ST	0.004
52	R-ST-0.4-14-3	MSA-14-3		0.004
53	R-ST-0.5-14-1	MSA-14-1		0.005
54	R-ST-0.5-14-2	MSA-14-2		0.005
55	R-ST-0.5-14-3	MSA-14-3		0.005
56	R-ST-0.6-14-1	MSA-14-1		0.006
57	R-ST-0.6-14-2	MSA-14-2		0.006
58	R-ST-0.6-14-3	MSA-14-3		0.006
59	R-ST-0.6-14-4	MSA-14-4		0.006
60	R-ST-0.7-14-2	MSA-14-2		0.007
61	R-ST-0.7-14-3	MSA-14-3		0.007
62	R-ST-0.7-14-4	MSA-14-4		0.007
63	R-ST-0.8-14-1	MSA-14-1		0.008
64	R-ST-0.8-14-2	MSA-14-2		0.008
65	R-ST-0.8-14-4	MSA-14-4		0.008
66	R-ST-0.9-14-1	MSA-14-1		0.009
67	R-ST-0.9-14-3	MSA-14-3		0.009
68	R-ST-0.9-14-4	MSA-14-4		0.009

Mix. No.	F-A mixture ID	PSD of coarse aggregate	Fiber type	V_f (m³/m³)
69	R-MiS-0.4-14-1	MSA-14-1	Micro steel	0.004
70	R-MiS-0.4-14-2	MSA-14-2		0.004
71	R-MiS-0.4-14-4	MSA-14-4		0.004
72	R-MiS-0.5-14-2	MSA-14-2		0.005
73	R-MiS-0.5-14-3	MSA-14-3		0.005
74	R-MiS-0.5-14-4	MSA-14-4		0.005
75	R-MiS-0.6-14-2	MSA-14-2		0.006
76	R-MiS-0.6-14-3	MSA-14-3		0.006
77	R-MiS-0.6-14-4	MSA-14-4		0.006
78	R-MiS-0.7-14-1	MSA-14-1		0.007
79	R-MiS-0.7-14-2	MSA-14-2		0.007
80	R-MiS-0.7-14-3	MSA-14-3		0.007
81	R-MiS-0.8-14-1	MSA-14-1		0.008
82	R-MiS-0.8-14-2	MSA-14-2		0.008
83	R-MiS-0.8-14-3	MSA-14-3		0.008
84	R-MiS-0.9-14-1	MSA-14-1		0.009
85	R-MiS-0.9-14-2	MSA-14-2		0.009
86	R-MiS-0.9-14-3	MSA-14-3		0.009
87	R-MiS-0.9-14-4	MSA-14-4		0.009
88	P-MiS-0.4-20-1	MSA-20-1		0.004
89	P-MiS-0.4-20-2	MSA-20-2		0.004
90	P-MiS-0.4-20-3	MSA-20-3		0.004
91	P-MiS-0.5-20-1	MSA-20-1		0.005
92	P-MiS-0.5-20-2	MSA-20-2		0.005
93	P-MiS-0.5-20-4	MSA-20-4		0.005

Table A3 (*continued*)

Mix. No.	F-A mixture ID	PSD of coarse aggregate	Fiber type	V_f (m^3/m^3)
94	P-MiS-0.6-20-1	MSA-20-1		0.006
95	P-MiS-0.6-20-2	MSA-20-2		0.006
96	P-MiS-0.6-20-3	MSA-20-3		0.006
97	P-MiS-0.6-20-4	MSA-20-4		0.006
98	P-MiS-0.7-20-1	MSA-20-1		0.007
99	P-MiS-0.7-20-2	MSA-20-2		0.007
100	P-MiS-0.7-20-3	MSA-20-3		0.007
101	P-MiS-0.7-20-4	MSA-20-4		0.007
102	P-MiS-0.8-20-1	MSA-20-1		0.008
103	P-MiS-0.8-20-3	MSA-20-3		0.008
104	P-MiS-0.8-20-4	MSA-20-4		0.008
105	P-MiS-0.9-20-1	MSA-20-1		0.009
106	P-MiS-0.9-20-2	MSA-20-2		0.009
107	P-MiS-0.9-20-3	MSA-20-3		0.009
108	P-MiS-0.9-20-4	MSA-20-4		0.009
109	R-IT-0.4-14-1	MSA-14-1	IT	0.004
110	R-IT-0.4-14-3	MSA-14-3		0.004
111	R-IT-0.4-14-4	MSA-14-4		0.004
112	R-IT-0.5-14-1	MSA-14-1		0.005
113	R-IT-0.5-14-2	MSA-14-2		0.005
114	R-IT-0.5-14-4	MSA-14-4		0.005
115	R-IT-0.6-14-2	MSA-14-2		0.006
116	R-IT-0.6-14-3	MSA-14-3		0.006
117	R-IT-0.6-14-4	MSA-14-4		0.006
118	R-IT-0.7-14-1	MSA-14-1		0.007
119	R-IT-0.7-14-2	MSA-14-2		0.007
120	R-IT-0.7-14-4	MSA-14-4		0.007
121	R-IT-0.8-14-1	MSA-14-1		0.008
122	R-IT-0.8-14-2	MSA-14-2		0.008
123	R-IT-0.8-14-3	MSA-14-3		0.008
124	R-IT-0.8-14-4	MSA-14-4		0.008
125	R-IT-0.9-14-2	MSA-14-2		0.009
126	R-IT-0.9-14-3	MSA-14-3		0.009
127	R-IT-0.9-14-4	MSA-14-4		0.009

Table A4
Proportioning and characteristics of F-A mixtures selected to validate the established DPD model (Eq. (9)).

Mix. No.	F-A mixture ID	Test- Sample	PSD of coarse aggregate in reference mixture	LPD$_{F-A}$	Fiber type	V_f in reference F-A mixture (m^3/m^3)	V_f in F-A sample mixture (m^3/m^3)
1	P-MaS-0.4-20-4	Reference	MSA-20-4	0.533	Macro steel	0.004	0.004
2	P-MaS-0.7-20-2		MSA-20-2	0.550		0.007	0.007
3	P-MaS-0.8-20-1		MSA-20-1	0.541		0.008	0.008
4	R-MaS-0.4-14-4		MSA-14-4	0.551		0.004	0.004
5	R-MaS-0.6-14-1		MSA-14-1	0.542		0.006	0.006
6	R-MaS-0.8-14-1		MSA-14-1	0.538		0.008	0.008
7	R-MaS-0.9-14-2		MSA-14-2	0.536		0.009	0.009
8	R-MaS-1.62-14-4		MSA-14-4	0.536		0.0162	0.0162
9	R-MaS-1.77-14-1		MSA-14-1	0.530		0.0177	0.0177
10	R-MaS-1.77-14-4		MSA-14-4	0.533		0.0177	0.0177
11	P-VP-33-MaS-0.4-20-4-L-E	L-Box - End	MSA-20-4	0.545		0.004	0.0030
12	P-VP-33-MaS-0.4-20-4-L-B	L-Box - Beginning	MSA-20-4	0.544		0.004	0.0052
13	P-VP-33-MaS-0.4-20-4-T-U	T-Box - Tilt-up	MSA-20-4	0.537		0.004	0.0024
14	P-VP-33-MaS-0.4-20-4-T-D	T-Box -Tilt-down	MSA-20-4	0.525		0.004	0.0058
15	P-VP-33-MaS-0.7-20-2-L-E	L-Box - End	MSA-20-2	0.518		0.007	0.0064
16	P-VP-33-MaS-0.7-20-2-L-B	L-Box - Beginning	MSA-20-2	0.530		0.007	0.0087
17	P-VP-33-MaS-0.7-20-2-T-U	T-Box - Tilt-up	MSA-20-2	0.523		0.007	0.0065
18	P-VP-33-MaS-0.7-20-2-T-D	T-Box -Tilt-down	MSA-20-2	0.533		0.007	0.0082
19	P-VP-33-MaS-0.5-20-3-L-E	L-Box - End	MSA-20-3	0.527		0.005	0.0047
20	P-VP-33-MaS-0.5-20-3-L-B	L-Box - Beginning	MSA-20-3	0.525		0.005	0.0054
21	P-VP-33-MaS-0.5-20-3-T-U	T-Box - Tilt-up	MSA-20-3	0.506		0.005	0.0045
22	P-VP-33-MaS-0.5-20-3-T-D	T-Box -Tilt-down	MSA-20-3	0.529		0.005	0.0058
23	P-VP-35-MaS-0.4-20-4-L-E	L-Box - End	MSA-20-4	0.509		0.004	0.0038
24	P-VP-35-MaS-0.4-20-4-L-B	L-Box - Beginning	MSA-20-4	0.491		0.004	0.0035
25	P-VP-35-MaS-0.4-20-4-T-U	T-Box - Tilt-up	MSA-20-4	0.511		0.004	0.0036
26	P-VP-35-MaS-0.4-20-4-T-D	T-Box -Tilt-down	MSA-20-4	0.529		0.004	0.0047
27	P-VP-35-MaS-0.7-20-2-L-E	L-Box - End	MSA-20-2	0.539		0.007	0.0072
28	P-VP-35-MaS-0.7-20-2-L-B	L-Box - Beginning	MSA-20-2	0.532		0.007	0.0080
29	P-VP-35-MaS-0.7-20-2-T-U	T-Box - Tilt-up	MSA-20-2	0.530		0.007	0.0068
30	P-VP-35-MaS-0.7-20-2-T-D	T-Box -Tilt-down	MSA-20-2	0.529		0.007	0.0087
31	P-VP-35-MaS-0.5-20-3-L-E	L-Box - End	MSA-20-3	0.516		0.005	0.0047

(*continued on next page*)

Table A4 (*continued*)

Mix. No.	F-A mixture ID	Test- Sample	PSD of coarse aggregate in reference mixture	LPD$_{F-A}$	Fiber type	V$_f$ in reference F-A mixture (m^3/m^3)	V$_f$ in F-A sample mixture (m^3/m^3)
32	P-VP-35-MaS-0.5-20-3-L-B	L-Box - Beginning	MSA-20-3	0.487		0.005	0.0062
33	P-VP-35-MaS-0.5-20-3-T-U	T-Box - Tilt-up	MSA-20-3	0.497		0.005	0.0044
34	P-VP-35-MaS-0.5-20-3-T-D	T-Box -Tilt-down	MSA-20-3	0.510		0.005	0.0067
35	P-VP-37-MaS-0.4-20-4-L-E	L-Box - End	MSA-20-4	0.542		0.004	0.0032
36	P-VP-37-MaS-0.4-20-4-L-B	L-Box - Beginning	MSA-20-4	0.545		0.004	0.0043
37	P-VP-37-MaS-0.4-20-4-T-U	T-Box - Tilt-up	MSA-20-4	0.544		0.004	0.0034
38	P-VP-37-MaS-0.4-20-4-T-D	T-Box -Tilt-down	MSA-20-4	0.537		0.004	0.0047
39	P-VP-37-MaS-0.7-20-2-L-E	L-Box - End	MSA-20-2	0.514		0.007	0.0063
40	P-VP-37-MaS-0.7-20-2-L-B	L-Box - Beginning	MSA-20-2	0.509		0.007	0.0081
41	P-VP-37-MaS-0.7-20-2-T-U	T-Box - Tilt-up	MSA-20-2	0.501		0.007	0.0063
42	P-VP-37-MaS-0.7-20-2-T-D	T-Box -Tilt-down	MSA-20-2	0.520		0.007	0.0086

Mix. No.	F-A mixture ID	Test- Sample	PSD of coarse aggregate in reference mixture	LPD$_{F-A}$	Fiber type	V$_f$ in reference F-A mixture (m^3/m^3)	V$_f$ in F-A sample mixture (m^3/m^3)
43	P-VP-37-MaS-0.5-20-3-L-E	L-Box - End	MSA-20-3	0.535	Macro steel	0.005	0.0036
44	P-VP-37-MaS-0.5-20-3-L-B	L-Box - Beginning	MSA-20-3	0.544		0.005	0.0060
45	P-VP-37-MaS-0.5-20-3-T-U	T-Box - Tilt-up	MSA-20-3	0.533		0.005	0.0034
46	P-VP-37-MaS-0.5-20-3-T-D	T-Box -Tilt-down	MSA-20-3	0.538		0.005	0.0058
47	R-VP-27-MaS-0.9-14-1-L-B	L-Box - Beginning	MSA-14-1	0.503		0.009	0.0118
48	R-VP-27-MaS-0.9-14-1-T-U	T-Box - Tilt-up	MSA-14-1	0.510		0.009	0.0089
49	R-VP-27-MaS-0.9-14-1-T-D	T-Box -Tilt-down	MSA-14-1	0.498		0.009	0.0108
50	R-VP-27-MaS-0.7-14-2-L-E	L-Box - End	MSA-14-2	0.524		0.007	0.0046
51	R-VP-27-MaS-0.7-14-2-L-B	L-Box - Beginning	MSA-14-2	0.521		0.007	0.0089
52	R-VP-27-MaS-0.7-14-2-T-U	T-Box - Tilt-up	MSA-14-2	0.519		0.007	0.0064
53	R-VP-27-MaS-0.7-14-2-T-D	T-Box -Tilt-down	MSA-14-2	0.521		0.007	0.0085
54	R-VP-27-MaS-0.4-14-3-L-E	L-Box - End	MSA-14-3	0.530		0.004	0.0035
55	R-VP-27-MaS-0.4-14-3-L-B	L-Box - Beginning	MSA-14-3	0.534		0.004	0.0051
56	R-VP-27-MaS-0.4-14-3-T-U	T-Box - Tilt-up	MSA-14-3	0.532		0.004	0.0038
57	R-VP-27-MaS-0.4-14-3-T-D	T-Box -Tilt-down	MSA-14-3	0.535		0.004	0.0049
58	R-VP-30-MaS-0.9-14-1-L-E	L-Box - End	MSA-14-1	0.516		0.009	0.0082
59	R-VP-30-MaS-0.9-14-1-L-B	L-Box - Beginning	MSA-14-1	0.496		0.009	0.0128
60	R-VP-30-MaS-0.9-14-1-T-U	T-Box - Tilt-up	MSA-14-1	0.505		0.009	0.0069
61	R-VP-30-MaS-0.9-14-1-T-D	T-Box -Tilt-down	MSA-14-1	0.508		0.009	0.0098
62	R-VP-30-MaS-0.7-14-2-L-E	L-Box - End	MSA-14-2	0.511		0.007	0.0060
63	R-VP-30-MaS-0.7-14-2-L-B	L-Box - Beginning	MSA-14-2	0.519		0.007	0.0071
64	R-VP-30-MaS-0.7-14-2-T-U	T-Box - Tilt-up	MSA-14-2	0.514		0.007	0.0057
65	R-VP-30-MaS-0.7-14-2-T-D	T-Box -Tilt-down	MSA-14-2	0.507		0.007	0.0089
66	R-VP-30-MaS-0.4-14-3-L-E	L-Box - End	MSA-14-3	0.525		0.004	0.0035
67	R-VP-30-MaS-0.4-14-3-L-B	L-Box - Beginning	MSA-14-3	0.533		0.004	0.0052
68	R-VP-30-MaS-0.4-14-3-T-U	T-Box - Tilt-up	MSA-14-3	0.532		0.004	0.0028
69	R-VP-30-MaS-0.4-14-3-T-D	T-Box -Tilt-down	MSA-14-3	0.529		0.004	0.0044
70	R-VP-33-MaS-0.9-14-1-L-E	L-Box - End	MSA-14-1	0.509		0.009	0.0083
71	R-VP-33-MaS-0.9-14-1-L-B	L-Box - Beginning	MSA-14-1	0.502		0.009	0.0118
72	R-VP-33-MaS-0.9-14-1-T-U	T-Box - Tilt-up	MSA-14-1	0.512		0.009	0.0060
73	R-VP-33-MaS-0.9-14-1-T-D	T-Box -Tilt-down	MSA-14-1	0.513		0.009	0.0111
74	R-VP-33-MaS-0.7-14-2-L-E	L-Box - End	MSA-14-2	0.525		0.007	0.0065
75	R-VP-33-MaS-0.7-14-2-L-B	L-Box - Beginning	MSA-14-2	0.529		0.007	0.0081
76	R-VP-33-MaS-0.7-14-2-T-U	T-Box - Tilt-up	MSA-14-2	0.527		0.007	0.0035
77	R-VP-33-MaS-0.7-14-2-T-D	T-Box -Tilt-down	MSA-14-2	0.506		0.007	0.0107
78	R-VP-33-MaS-0.4-14-3-L-E	L-Box - End	MSA-14-3	0.535		0.004	0.0036
79	R-VP-33-MaS-0.4-14-3-L-B	L-Box - Beginning	MSA-14-3	0.533		0.004	0.0043
80	R-VP-33-MaS-0.4-14-3-T-U	T-Box - Tilt-up	MSA-14-3	0.534		0.004	0.0029
81	R-VP-33-MaS-0.4-14-3-T-D	T-Box -Tilt-down	MSA-14-3	0.541		0.004	0.0054

Mix. No.	F-A mixture ID	Test- Sample	PSD of coarse aggregate in reference mixture	LPD$_{F-A}$	Fiber type	V$_f$ in reference F-A mixture (m^3/m^3)	V$_f$ in F-A sample mixture (m^3/m^3)
82	P-MiS-0.4-20-4	Reference	MSA-20-4	0.563	Micro steel	0.004	0.004
83	P-MiS-0.5-20-3		MSA-20-3	0.565		0.005	0.005
84	P-MiS-0.8-20-2		MSA-20-2	0.563		0.008	0.008
85	R-MiS-0.4-14-3		MSA-14-3	0.556		0.004	0.004
86	R-MiS-0.5-14-1		MSA-14-1	0.559		0.005	0.005
87	R-MiS-0.6-14-1		MSA-14-1	0.550		0.006	0.006
88	R-MiS-0.7-14-4		MSA-14-4	0.554		0.007	0.007
89	R-MiS-0.8-14-4		MSA-14-4	0.553		0.008	0.008
90	R-ST-0.4-14-1		MSA-14-1	0.546	ST	0.004	0.004
91	R-ST-0.4-14-4		MSA-14-4	0.553		0.004	0.004
92	R-ST-0.5-14-4		MSA-14-4	0.551		0.005	0.005
93	R-ST-0.7-14-1		MSA-14-1	0.539		0.007	0.007
94	R-ST-0.8-14-3		MSA-14-3	0.542		0.008	0.008
95	R-ST-0.9-14-2		MSA-14-2	0.538		0.009	0.009
96	R-IT-0.4-14-2		MSA-14-2	0.548	IT	0.004	0.004
97	R-IT-0.5-14-3		MSA-14-3	0.555		0.005	0.005
98	R-IT-0.6-14-1		MSA-14-1	0.540		0.006	0.006
99	R-IT-0.7-14-3		MSA-14-3	0.547		0.007	0.007
100	R-IT-0.9-14-1		MSA-14-1	0.536		0.009	0.009

References

[1] A. Emdadi, I. Mehdipour, N.A. Libre, M. Shekarchi, Optimized workability and mechanical properties of FRCM by using fiber factor approach: theoretical and experimental study, Mater. Struct. 48 (4) (2015) 1149–1161, https://doi.org/10.1617/s11527-013-0221-3.

[2] Y. Lu, Z. Liu, S. Li, W. Li, Behavior of steel fibers reinforced self-stressing and self-compacting concrete-filled steel tube subjected to bending, Constr. Build. Mater. 156 (2017) 639–651, https://doi.org/10.1016/j.conbuildmat.2017.09.019.

[3] X. Ning, Y. Ding, F. Zhang, Y. Zhang, Experimental study and prediction model for flexural behavior of reinforced SCC beam containing steel fibers, Constr. Build. Mater. 93 (2015) 644–653, https://doi.org/10.1016/j.conbuildmat.2015.06.024.

[4] E.V. Sarmiento, G. Zirgulis, S. Sandbakk, M.R. Geiker, T. Kanstad, Influence of concrete flow on fibre distribution, orientation and mechanical properties of fibre reinforced concrete, in: 8th RILEM International Symposium on Fiber Reinforced Concrete: challenges and opportunities, BEFIB 2012, 2012, pp. 418–430.

[5] K.M.A. Hossain, M. Lachemi, M. Sammour, M. Sonebi, Influence of polyvinyl alcohol, steel, and hybrid fibers on fresh and rheological properties of self-consolidating concrete, Mater. Civil Eng. 24 (9) (2012) 1211–1220, https://doi.org/10.1061/(ASCE)MT.1943-5533.0000490.

[6] I. Mehdipour, N.A. Libre, Linking fiber factor to material performance of fiber reinforced self-consolidating cement-based materials, ACI Mater. J. 114 (1) (2017) 77–91, https://doi.org/10.14359/51689483.

[7] I. Mehdipour, N.A. Libre, M. Shekarchi, M. Khanjani, Effect of workability characteristics on the hardened performance of FRSCCMs, Constr. Build. Mater. 40 (2013) 611–621, https://doi.org/10.1016/j.conbuildmat.2012.11.051.

[8] M. Nehdi, J.D. Ladanchuk, Fiber synergy in fiber-reinforced self-consolidating concrete, ACI Mater. J. 101 (6) (2004) 508–517, https://doi.org/10.14359/13490.

[9] A.S. El-Dieb, M.M.R. Taha, Flow characteristics and acceptance criteria of fiber-reinforced self-compacted concrete (FR-SCC), Constr. Build. Mater. 27 (1) (2012) 585–596, https://doi.org/10.1016/j.conbuildmat.2011.07.004.

[10] K.H. Khayat, F. Kassimi, P. Ghoddousi, Mixture design and testing of fiber-reinforced self-consolidating concrete, ACI Mater. J. 111 (2) (2014) 143, https://doi.org/10.14359/51686722.

[11] M. Hosseinpoor, B.I.O. Koura, A. Yahia, Rheo-morphological investigation of static and dynamic stability of self-consolidating concrete: A biphasic approach, Cem. Concr. Compos. 121 (2021), 104072, https://doi.org/10.1016/j.cemconcomp.2021.104072.

[12] M. Hosseinpoor, B.I.O. Koura, A. Yahia, New diphasic insight into the restricted flowability and granular blocking of self-consolidating concrete: Effect of morphological characteristics of coarse aggregate on passing ability of SCC, Constr. Build. Mater. 308 (2021), 125001, https://doi.org/10.1016/j.conbuildmat.2021.125001.

[13] B.I.O. Koura, M. Hosseinpoor, A. Yahia, Coupled effect of fine mortar and granular skeleton characteristics on dynamic stability of self-consolidating concrete as a diphasic material, Constr. Build. Mater. 263 (2020) 120–131, https://doi.org/10.1016/j.conbuildmat.2020.120131.

[14] A.K.H. Kwan, K.W. Chan, V. Wong, A 3-parameter particle packing model incorporating the wedging effect, Powder Technol. 237 (2013) 172–179, https://doi.org/10.1016/j.powtec.2013.01.043.

[15] L.G. Li, Z.W. Zhao, J. Zhu, A.K.H. Kwan, K.L. Zeng, Combined effects of water film thickness and polypropylene fibre length on fresh properties of mortar, Constr. Build. Mater. 174 (2018) 586–593.

[16] L.G. Li, J. Zhu, Z.W. Zhao, A.K.H. Kwan, Roles of water film thickness and polypropylene fibre content in fresh properties of mortar, Adv. Cem. Res. 29 (2) (2017) 71–80, https://doi.org/10.1680/jadcr.16.00102.

[17] G. Sokhansefat, M.T. Ley, M.D. Cook, R. Alturki, M. Moradian, Investigation of concrete workability through characterization of aggregate gradation in hardened concrete using X-ray computed tomography, Cem. Concr. Compos. 98 (2019) 150–161, https://doi.org/10.1016/j.cemconcomp.2019.02.008.

[18] K. Molugaram, J.S. Shanker, A. Ramesh, A study on influence of shape of aggregate on strength and quality of concrete for buildings and pavements, Adv. Mater. Res. 941–944 (2014) 776–779, https://doi.org/10.4028/www.scientific.net/AMR.941-944.776.

[19] K. Ostrowski, L. Sadowski, D. Stefaniuk, D. Walach, T. Gawenda, K. Oleksik, I. Usydus, The effect of the morphology of coarse aggregate on the properties of self-compacting high-performance fiber-reinforced concrete, Materials 11 (2018) 1–16, https://doi.org/10.3390/ma11081372.

[20] B.M. Aissoun, S.D. Hwang, K.H. Khayat, Influence of aggregate characteristics on workability of superworkable concrete, Mater. Struct. 49 (2016) 597–609, https://doi.org/10.1617/s11527-015-0522-9.

[21] R. Farokhzad, M. Mahdikhani, A. Bagheri, J. Baghdadi, Representing a logical grading zone for self-consolidating concrete, Constr. Build. Mater. 115 (2016) 735–745, https://doi.org/10.1016/j.conbuildmat.2016.04.006.

[22] H. Hafid, G. Ovarlez, F. Toussaint, P.H. Jezequel, N. Roussel, Effect of particle morphological parameters on sand grains packing properties and rheology of model mortars, Cem. Concr. Res. 80 (2016) 44–51, https://doi.org/10.1016/j.cemconres.2015.11.002.

[23] L. Martinie, P. Rossi, N. Roussel, Rheology of fiber reinforced cementitious materials: classification and prediction, Cem. Concr. Res. 40 (2) (2010) 226–234, https://doi.org/10.1016/j.cemconres.2009.08.032.

[24] S.H. Chu, Y. Jiang, A.K.H. Kwan, Effect of rigid fibres on aggregate packing, Constr. Build. Mater. 224 (2019) 326–335, https://doi.org/10.1016/j.conbuildmat.2019.07.072.

[25] F. de Larrard, Concrete mixture proportioning - a scientific approach, in: S. Mindess, A. Bentur (Eds.), Modern Concrete Technology Series No. 7, E&FN SPON, London (1999) ISBN 9780419235002.

[26] N. Roussel, Understanding the Rheology of Concrete, first ed., Woodhead Publishing, Sawston, Cambridge, United Kingdom, 2011.

[27] A.B. Yu, R.P. Zou, Prediction of the porosity of particle mixtures, Kona Powder Part. J. 16 (1998) 68–81, https://doi.org/10.14356/kona.1998010.

[28] Z.S. Ali, M. Hosseinpoor, A. Yahia, New aggregate grading models for low-binder self-consolidating and semi-self-consolidating concrete (Eco-SCC and Eco-semi-SCC), Constr. Build. Mater. 265 (2020), 120314, https://doi.org/10.1016/j.conbuildmat.2020.120314.

[29] M. Hosseinpoor, B.I.O. Koura, A. Yahia, Rheo-morphological investigation of Reynolds dilatancy and its effect on pumpability of self-consolidating concrete, Cem. Concr. Compos. 117 (2021), 103912, https://doi.org/10.1016/j.cemconcomp.2020.103912.

[30] Nordtest, Method (NT BUILD 427) for Fresh Concrete: Compatibility with IC-tester (Intensive Compaction Tester) Proj. 1005-91, Nord. Scand. Inst. (1994) 1-4, ISSN 0283-7153 www.nordtest.org.

[31] B.M. Aïssoun, Method (NT BUILD 427) for Fresh Concrete: Compatibility on the rheology of fluid concrete with adapted rheology (in French), M.Sc. thesis, Université de Sherbrooke, 2011 http://savoirs.usherbrooke.ca/handle/11143/1590.

[32] B.I.O. Koura, M. Hosseinpoor, A. Yahia, E.H. Kadri, A. Kaci, A new proportioning approach of low and normal binder self-consolidating concrete based on the characteristics of fine mortar and granular skeleton, Constr. Build. Mater. 239 (2020), 117892, https://doi.org/10.1016/j.conbuildmat.2019.117892.